STRUCTURE-PROPERTY RELATIONSHIPS IN 4D-PRINTED LIQUID CRYSTAL ELASTOMERS

By

ZOZEF SIDDIQUI
Bachelor of Science in Mechanical Engineering
Bangladesh University of Engineering and Technology
Dhaka, Bangladesh
2017

Submitted to the Faculty of the
Graduate College of the
Oklahoma State University
in partial fulfillment of
the requirements for
the Degree of
Master of Science
MAY, 2021

STRUCTURE-PROPERTY RELATIONSHIPS
IN 4D-PRINTED LIQUID CRYSTAL
ELASTOMERS

Dissertation Approved:

Dr. Aurelie Azoug

Dissertation Advisor

Dr. James E. Smay

Dr. Sandip Harimkar

ACKNOWLEDGMENTS

First of all, I would like to thank my advisor Dr. Azoug for her mentoring and support. This research work would not have been possible without her guidance and assistance. She granted me a comfortable amount of freedom and often challenged my views to grow my knowledge. Furthermore, I want to thank to my committee members Dr. Smay and Dr. Harimkar for their suggestions and help to perform my research work.

I would also like to thank my colleagues and friends for the challenging discussions we had as well as their support during and after working hours. Their constructive criticism and insight regarding my research helped me overcome a lot of sticking points in my research.

Finally, I am deeply indebted to my father Rahmat Ali Siddiqui and my mother Afroza Siddiqui as well as my sister Ria Siddiqui for their unconditional trust and support. I am lucky to have them on my side and I wouldn't be where I am now without their encouragement to pursue my dreams against all odds.

Acknowledgments reflect the views of the author and are not endorsed by committee members or Oklahoma State University.

Name: ZOZEF SIDDIQUI

Date of Degree: MAY, 2021

Title of Study: STRUCTURE-PROPERTY RELATIONSHIPS IN 4D-PRINTED LCE

Major Field: MECHANICAL AND AEROSPACE ENGINEERING

Abstract:

Liquid Crystal Elastomers (LCEs) are active smart materials that exhibit reversible shape changes, or actuation, via the transition between the nematic or liquid crystal state and the isotropic state with the application of heat, light, magnetic field, etc. 4D printing is a form of 3D printing involving smart materials and allows for a change in shape in the post-fabrication phase. The current 4D printing techniques rely predominantly on structure and often on multi-material printing. In this study, we explored the actuation and the viscoelastic mechanical behavior of single-material (LCE) 3D-printed structures, controlling printing parameters such as printing speed, printing angle, etc.

The actuation strain of 4D-printed LCEs increases with the printing speed, reaching as high as 42%. In addition, 4D-printed LCEs tend to bend more when printed at higher printing angles. Young's, storage, and loss moduli increase with printing speed up to a threshold, where the quality of the print decreases. We also found that 4D-printed LCEs exhibit higher moduli than bulk LCEs, due to liquid crystals alignment. Young's, storage, and loss moduli decrease with the printing angle, showing the influence of the liquid crystal preferred direction on the mechanical properties. By precisely regulating printing speed and angle, we fabricated- 2D contracting grids, functional hinges, self-folding boxes, 2D rectangles becoming 3D pyramids and ribbons turning into 3D helices.

These results show the potential of additively-manufactured heat-responsive LCEs capable of reversibly actuating between two pre-programmed shapes for applications in soft robotics, biomedical prosthetics and implants, dynamic functional architecture, etc.

TABLE OF CONTENTS

LIST OF FIGURES

CHAPTER I

Introduction and General Background

1.1 4D printing

1.1.1 Definition

The technique of 4D-printing designates the additive manufacturing of a smart material system that can change shape in the post-fabrication phase, where the fourth dimension is the time [7]. The 4D printing technology is based on 3D printing, but requires additional stimulus and stimulus-responsive materials to facilitate shape change after manufacturing. 3D printing deals with static objects where as 4D printing allows a dynamic change in configuration in 3D printed objects in response to external stimuli such as heat [8, 9], light [10, 11], water [12, 1], etc. objects manufactured by 4D printing exhibit an intelligent time-dependent behavior based on various interaction mechanisms among smart materials, various stimulus, material programming, and mathematical modeling [13].

The main components of 4D printing are a 3D printing facility, a smart or stimulus-responsive material, an external stimulus and a mathematical modeling for material programming.

1.1.2 3D Printing Technique

The first component, a 3D printing facility, refers to a wide range of 3D printing apparatus and techniques, such as direct ink writing (DIW) [14], fused deposition modeling (FDM) [10], stereolithography (SLA) [15], selective laser sintering (SLS) [16], which can all be used for the purpose of 4D printing. The printing parameters of any setup have a large influence on the obtained product. Changing a printing parameter, like printing speed or printing temperature [17], can affect the degree of post-manufacturing shape change of the 4D printed object.

Fused Deposition Modeling (FDM)

Extrusion-based 3D printing techniques can be used to 4D print shape-memory polymers. In an extrusion-based printing method, material is selectively dispensed on the printing bed through a nozzle or orifice. The most popular and common form of extrusion-based printing is FDM where thermoplastic filaments are extruded through a heated nozzle in order to melt and deposit the material layer by layer on a build platform.

FDM printing method can be used in single-step fabrication processes to print various in-plane structures with polymers like PLA (Polylactic acid), ABS(Polylactic acid), etc. [18].

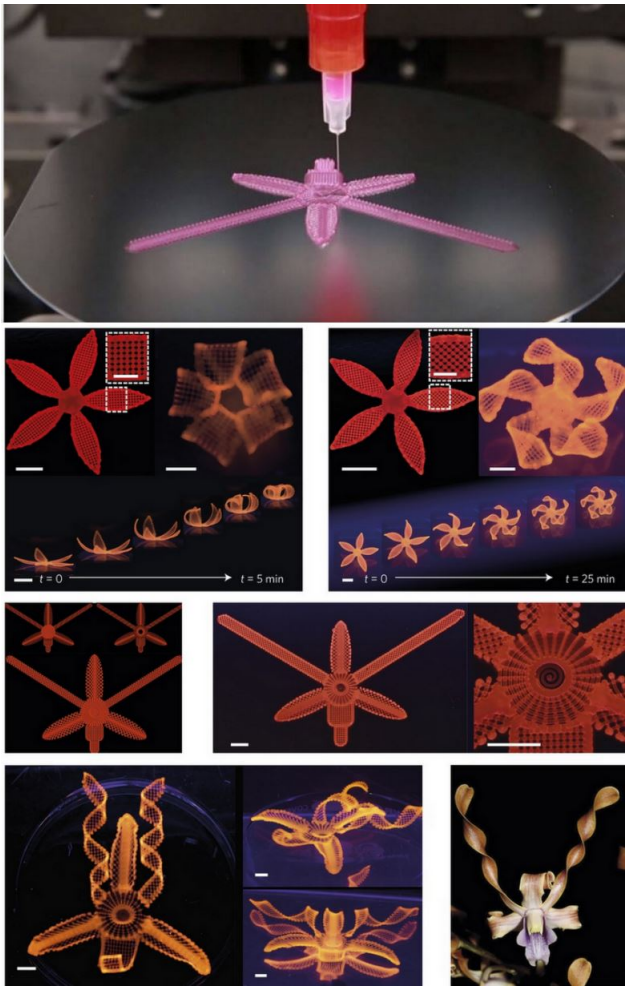

Figure 1: 4D printing of a bio-mimetic flower and its post manufacturing shape change [1]

For this purpose, the PLA or ABS filament is stretched during printing at a temperature above its melting point (T_m) which causes visible alignment of the polymer chains along the extrusion direction. Component porosity, filament plying angle, layer height, etc., are the printing parameters used in order to regulate the shrinking behavior of the printed structure.

Direct Ink Writing (DIW)

DIW is an extrusion-based additive manufacturing method where the printing ink is dispensed in liquid phase under a controlled flow rate through a small nozzle and the ink is deposited along digitally defined paths to additively manufacture structures layer-by-layer [19]. DIW printing method is compatible with a wide range of materials including metal particles [20], polymers [21], ceramics [22], multimaterial [23], etc. The ink used in DIW printing is viscoleastic possessing both shear thinning characteristics and a rapid pseudo-elastic behavior [24, 25]. Shear thinning in DIW takes place when the viscosity of the ink decreases with the increase in shear force inside the nozzle which allows the extrusion of the ink through the fine orifice. When the ink comes out of the nozzle, high shear elastic modulus and high shear yield strength are regained as the shear force on the ink decreases

abruptly. This is how the ink remains in filamentary shape after the hot extrusion which is required to construct a complex shape.

Stereolithography (SLA) and projection microstereolithography (PμSL)

SLA is one of the oldest 3D printing methods, using photopolymers to create highly complex shapes with micrometer precision. In the SLA process, liquid photo-sensitive resins or polymers are cured by laser treatment to form a solidified shape [15]. The use of SLA is hence limited to photocurable materials. Shape memory polymers (SMP) have to be highly stretchable at temperatures above their transition temperature to allow for a large shape change. But many 3D printable photopolymers lack stretchability due to their high cross-linking density which renders them not suitable for 4D printing via SLA. The projection microstereolithography (PμSL) method, which is a more precise version of the SLA method, can be used to improve the stretchability of SMPs [2]. Methacrylate-based copolymer networks and several difunctional acrylate oligomers can be used to prepare this highly tailorable SMP and these tweaks increases the rubbery modulus from about 1 to 100 MPa, glass transition temperature (T_g) from 50 to 180°C, and the failure strain up to about 300% [2]. Using this methacrylate-based copolymer, a bent model of the Eiffel tower was printed that would straighten up to resemble the Eiffel tower with the application of heat (Fig. 2). The SLA method can be used to print tBA-co-DEGDA networks with complex geometries where shape change is based on the dual-component phase switching mechanism [15]. These 4D printed SMP parts exhibit 82% higher elongation in their rubbery state than conventionally manufactured industrial grade thermoset SMPs. Polyurethane acrylate can

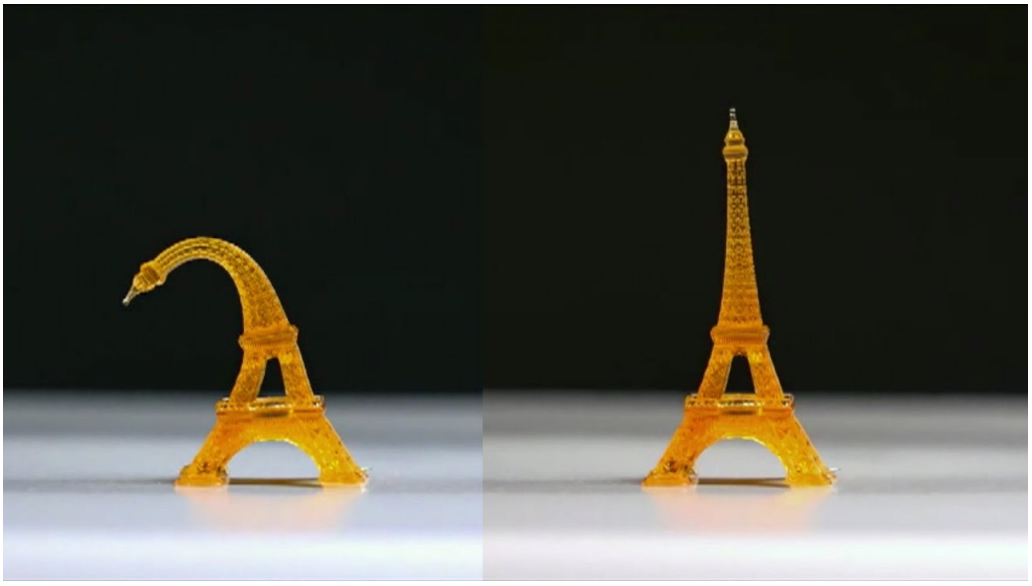

Figure 2: 4D printed bent Eiffel tower that straightens with the application of heat [2]

be compounded with epoxy acrylate, isobornyl acrylate, and radical photoinitiator to get a photopolymer suitable for SLA printing [26]. Fold-deploy test and shape-memory cycles measurements show that polyurethane acrylate-based 4D printed materials show excellent

shape-memory performance as they have almost 100% recovery ratio and 97% shape fixity [26].

Digital Light Processing (DLP)

DLP is a 3D printing process similar to SLA where a projector is used instead of a UV laser to selectively solidify liquid photocurable resins layer-by-layer. With the DLP method, an entire layer can be cured at one time in a matter of a few seconds without the need for any additional supporting structure [27]. Zhao et al. [28] used DLP to create complicated, reversible, free-standing origami structures. Using gray-scale patterned light and photoabsorbers, the light intensity can be controlled even more precisely along the thickness axis.

Huang et al. [29] demonstrated a very fast DLP varying the exposure time of light on different regions of a two dimensional sheet. The photocured 4D printed polymer had different levels of cross-linking density and monomer conversion in the different regions. Then, when water was added to the cured material, different degrees of swelling was observed as the sheet had site-specific monomer desolvation properties and cross-linking density. The 2D sheet assumed a 3D shape as gradients of internal stresses were introduced by the swelling difference at different positions.

DLP has also been used to manufacture 4D printed composite hydrogels. Hydrogels can expand up to twice their original volume by absorbing moisture but their major problem is that the reverse process, i.e. shrinking by drying, is 10-13 times slower than the swelling process [30].

1.1.3 Printed Materials

The second component of 4D printing is the printed material. Although 4D printing is often purely defined as the printing of a stimulus- responsive or smart material, there have efforts to reach similar shape-changing properties with standard polymers. Nonetheless, materials with shape- memory properties are ideal for 4D printing.

Shape-Memory Polymers (SMPs)

Both shape-memory materials and shape-changing materials can be used for the purpose of 4D printing. A shape-changing material changes its shape with the application of stimulus and returns to its permanent shape immediately with the removal of the stimulus. On the other hand, shape-memory materials are programmed to a deformed shape from their primary shape and held in this temporary semi-stable shape. They finally recover to the original shape with the application of a stimulus [31, 32]. Shape-memory polymers (SMPs) are smart polymer materials that can be inelastically deformed and then reverted to their original shape by an external stimulus and thus they exhibit the shape-memory effect (SME) [33, 34]. With a few exceptions, the actuation of SMPs is generally not reversible, meaning the actuation can only happen once before reprogramming is needed [33].

Internal Stress Release

The shape programming step for the 4D printing of SMPs can be bypassed with the utilization of heat-shrinkable properties [35]. In this strategy, polymer is heated above its glass transition temperature (T_g) which releases the internal strain energy induced in the polymer due to the extrusion during the 3D printing process. Using this strategy, Zhang et al. printed a 2D PLA lattice that could undergo a controlled, sequential folding and unfolding and create flower-like patterns [35]. The heat shrinkage of printed polymer can be further combined with geometry control to enable more complex shape-morphing behaviors in objects printed via extrusion-based printing techniques.

Heat activated SMPs can also be indirectly heated via photo induced heating. Liu et al. used an FDM printer to deposit inks of different light absorptivity on homogeneously pre-strained polystyrene sheets [36]. The different colored inks on the surface of the sheets absorbed light discriminatively on the basis of the color of the ink and the wavelength of the incident light. The pre-strained polystyrene sheet got heated up by the light absorbed by the ink, which led to the release of strain and the triggering of the folding mechanism. In this way, sequential folding of a 3D printed object can be achieved via the regulation of the incident light wavelength and the ink color.

1.1.4 Stimulus

The external stimulus component basically refers to the various stimuli that trigger the shape change in smart materials. Some smart materials have the ability to change their shape in response to specific stimuli, like heat, water, pH level, magnetic field, electric field, etc. Yang et al. reported the 3D printing of shape-memory polymers by combining FDM printing technology and photothermal effect of carbon black–reinforced polyurethane, where sunlight triggered the shape-memory behavior of the printed material [10]. Wei et al. used extrusion based additive manufacturing of poly-lactic acid PLA/Fe_3O_4 composite inks to produce remotely controllable 4D printed SMP where a magnetic field could heat Fe_3O_4 nanoparticles remotely and trigger the shape-memory effect [37]. In case of multi-material 4D printing, the different material responses of different materials to a stimulus can lead to complicated shape-morphings [38].

1.1.5 Mathematical Modeling and Shape-change Programming

The final component of 4D printing is the mathematical modeling necessary to program complex shape changes in the printed system, basically priming the material for post-fabrication shape change. The shape changes in 4D-printed objects are predictable and programmable. By controlling the various printing parameters, printing shape, deposition of the material, certain shape change commands are programmed into the material during printing and this programming, in turn, leads to a pre-determined change in shape [13]. In order to design complex changes in shape, extensive mathematical modeling is required. 4D printing facilitates a very wide range of shape-shifting patterns including linear or nonlinear expansion and contraction, folding, bending, twisting, surface curling, 1D to 1D, 1D to 2D, 2D to 2D, 1D to 3D, 2D to 3D, and 3D to 3D deformation. Surface topographical features like wrinkles, buckles, and creases can also be generated with 4D printing.

1D to 1D

Raviv et al. reported 1D to 1D deformation using 4D printed hydrogels [12] where the structure consisted of stacked layers of hydro-responsive active materials and rigid polymers. When immersed in water, the hydrogel parts swelled while the rigid discs remained unchanged. The structure exhibited linear shape-shifting behavior with a pre-programmed final length as composition of active hydrogels and rigid discs was varied.

1D to 2D

Tibbits demonstrated 1D to 2D shape-shifting self-folding mechanism by printing a line-shaped structure that could bends and twists to form the letters "MIT" in an aqueous environment as shown in figure 3 [3]. The structure consisted of two materials: a hydro-responsive active materials and a passive rigid material.

Figure 3: Example of a 1D to 2D deformation of a 4D printed material [3]

2D to 2D

An example of in-plane shape shifting can be the bending of a rectangular shape into a circular shape as shown in figure 4 where the active materials are 4D printed active droplets [4]. This shape-shifting behavior is triggered by the difference in osmotic concentration in the droplets. Swelling happens to the droplets with higher osmotic concentration and shrinkage happens to the droplets with lower osmotic concentration. The continuous shrinkage and expansion leads to the shape change in the structure from rectangular to circular. The same material and principle can be used to print a two-dimensional flower-shaped structure capable of transforming into a spherical shape [4].

2D to 3D

Tibbits et al. (2014) showed an example of surface topographical shape-shifting (2D plane to 3D shape) by generating mountain and valley-like features from concentric circles. This shape-shifting behavior was triggered by the actuation of the active materials and took

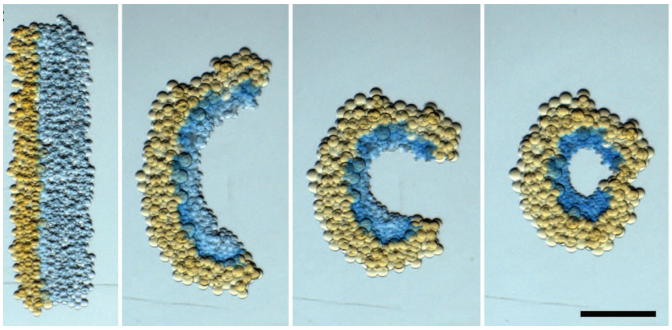

Figure 4: Photographs of a rectangular network folding into a circle (2D to 2D deformation). Scale bar is 250 μm. [4]

advantage of the stress mismatch between passive and active materials that arose from their different swelling properties in water.

Printing fibers at a certain angle can induce twisting mechanism in a 4D printed object. For example, obliquely printed overlapping fibers can lead to twisting that can transform a flat sheet to a 3D spiral [39]. Gladman et al. illustrated combined bending and twisting behaviors by printing a 2D floral shaped sheet morphing into a 3D flower [1]. Composite hydrogel architectures were printed that were encoded with localized, anisotropic swelling behavior controlled by the alignment of cellulose fibrils along the 3D printing pathways. The active hydrogel swelled in contact with water but the rigid materials in the structure remained unchanged and thus the structure attained a 3D flower shape as shown in figure 1.

1.1.6 Future Application

As a nascent technology, the applications of 4D printing outside the scope of a laboratory is not yet as prominent. But the potential applications of this sophisticated technology have attracted a lot of research interest in recent times.

Self-assembly

Instead of additively manufacturing a complicated structure in one go, simple components can be 3D printed one at a time with smart materials and then those components can self-assemble to attain the desired complex shape [31]. One potential use of self-assembly can be the transfer of small bio-mechanical parts inside the human body and then those tiny parts can assemble by themselves at the desired location to form a device and serve bio-medical purposes [31]. The self-assembling feature of 4D printed objects can further be utilized while erecting buildings and manufacturing machine parts in hard-to-reach areas like war zones, bio-hazard zones, and even outer space, where the part-by-part manufactured fragments of a bigger structure can self-assemble bypassing the risk of human involvement [7].

Self-adaptability

Another potential application of 4D printing can be self-adaptability. In a 4D printed structure, the material itself serves the purpose of sensing and, actuation which was traditionally incorporated in structures via electronic or mechanical systems [3]. As these systems are

redundant in 4D printed assemblies, a smaller number of parts are is required for a fully functional structure. These simpler designs can significantly reduce the time, energy, and expenses required for manufacturing and assembly. 4D printed muscle tissues [40, 41] and 4D-printed custom-made individualized artificial bio-parts, like tracheal stents [42], are potential applications of the self-adaptability feature of 4D printed materials.

Self-healing

4D printed materials exhibit self-repair potential as well. The self-repairing and error-correct capability of 4D manufactured products can ensure reusability and better recycling [3]. The self-repair feature of 4D printed objects have already been exploited in self-healing pipes [7] and self-healing hydrogels [43] and it has potential to be used as bio-parts.

1.2 Liquid Crystal Elastomers

Liquid Crystal Elastomers (LCEs) are active materials that exhibit two-way shape changes via the transition between the nematic or liquid crystal state and the isotropic state [44] with the application of heat [45] , light [46], or a solvent [47]. LCEs challenge the traditional classifications of materials as the liquid crystals exhibit extraordinary properties when integrated in a polymer network, including soft elasticity, two-way actuation and mechanical and optical anisotropic responses [48]. LCEs have often been deemed as a whole new state of matter because they sometimes behave like a solid, sometimes like a liquid [49].

1.2.1 Composition

LCEs are mildly crosslinked liquid crystal polymer networks and their properties combine the elasticity of elastomer chains and the self-organization of liquid crystals known as mesogens [50].

Mesogens

Mesogens are molecules with an elongated and anisotropic shape that tend to order themselves with respect to each other. The mesogen's self-organizing behavior allows LCEs to remain ordered even in a semi-fluid state [51]. The mesogens also have easily polarizable dipoles, a strong backbone core consisting of 2-3 aromatic rings linked together, and double bonds in the long axis. The flexible ends let the mesogens reorient themselves seamlessly [52]. The arrangement and shape of the aromatic rings in the mesogen have a strong influence on the dielectric and birefringence properties of the LCE [53].

Polymer network

Mesogens are separated by polymer chains called spacers and polymer crosslinkers to form the LCE network. The specific volume of the entire network is usually less than the specific volume of the mesogen monomers. The reduced free volume transfers the LC phase regime of the polymer towards a higher temperatures. Thus, LCEs show solid-like behavior unlike other low molar mass liquid crystals with similar chemical constitution [5].

The mesogens can connect to the polymer chain in three different ways [5]. First is the main chain LCE where the mesogens are directly connected to the polymer backbone via the long axis. The mesogens can be connected to the main chain by their ends or their sides (Figure 5). Second is the side chain LCE where the mesogens are linked to the polymer backbone with a short spacer. The mesogens can be linked to the spacer by their ends or sides (Figure 5). The LCE anisotropy and nematic phases largely depend upon the mesogen-

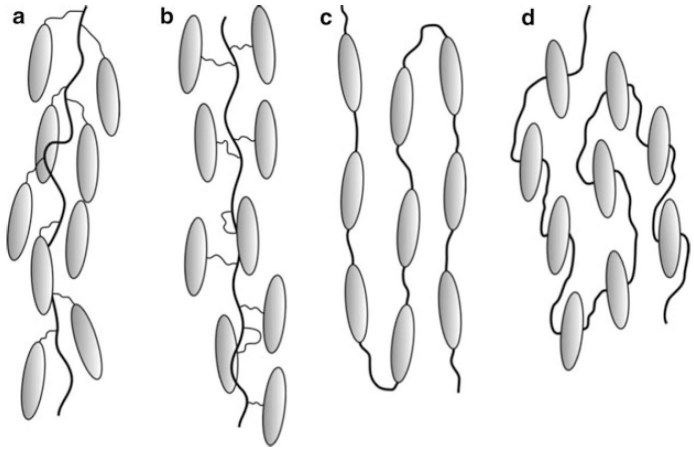

Figure 5: Different types of attachment geometries for the mesogens of an LCE chain: side chain elastomers with mesogens connected to the spacer by their ends (a) or sides (b) and main chain elastomers with mesogenic units connected to the main chain by their ends (c) or sides (d) [5]

backbone attachment type [54, 55]. But after alignment, the classical isotropic spherical coil formed by the undisturbed polymer chain distorts into an elongated spheroid shape [5].

Influence of synthesis

The synthetic history of an LCE controls its macroscopic behavior, meaning the presence or absence of liquid crystal order during synthesis can influence the behavior of the synthesized material [56]. Using solvents to melt the mesogens during synthesis provides multiple advantages, like the ability to synthesize LCEs at room temperature and the reduced viscosity leading to easier handling [57]. However, using a solvent can be disadvantageous as the mesogen order is lost and an isotropic solution is formed before crosslinking [56]. However, this influence is limited if the solution is heated above the nematic-isotropic transition temperature (T_{NI}) during synthesis, that is if the synthesis is performed in the isotropic phase [5]. Moreover, the solvent needs to be forcefully drawn out of the LCE after the crosslinking phase, usually via evaporation, which can be time-consuming and result in shrinkage or surface irregularities. Instead of using solvents, melting the mesogens keeps the mesogen order without the need for an extra evaporation step after crosslinking [56]. This process needs to be carried out at a higher temperature, which can restrict the use of a whole array of crosslinkers and spacers. The synthesis temperature should be above the melting temperature of the pure mesogens but below the T_{NI} to preserve the liquid crystal order [56].

1.2.2 Phases and Transition Temperatures

Nematic and isotropic phases

The LCEs transitions determine their domain of usability and functionality. LCEs exhibit three phases: glassy, nematic, and isotropic. The glassy phase is common to all polymers and corresponds to a decrease in molecular mobility below the glass transition temperature (T_g). The nematic phase is the liquid crystal phase and corresponds to the phase in which mesogens can form ordered structures. At the nematic-isotropic transition temperature (T_{NI}), the liquid crystals melt, that is the mesogens disorder to form an isotropic phase.

Three categories of mesogens are defined by the stimulus required to trigger the nematic-isotropic transition: thermotropic, lyotropic, and metallotropic [48].

- Thermotropic liquid crystals usually consist of organic materials, and the phase transition behavior is mainly regulated by temperature [51].
- Lyotropic liquid crystals primarily consists of amphiphilic mesogens and their phase transition depends on temperature and the concentration of the mesogens [58].
- Metallotropic liquid crystals contain both inorganic and organic molecules and their phase transition depends on the concentration of mesogens, temperature, and the proportion of inorganic and organic molecules [59].

We will concentrate on thermotropic liquid crystals because they are the most common and the ones used in this study.

Polydomain and monodomain phases

When a liquid crystal elastomer is at room temperature and not stretched, it is commonly in the polydomain state and looks opaque and white. In the polydomain state, the mesogens are locally ordered in sub-domains but the material remains macroscopically isotropic. If heated, the polydomain LCE shifts to the isotropic state and appears transparent as mesogens are disordered and the elastomer is amorphous [60]. The isotropic material reverts back to polydomain upon cooling. There is no change in shape during the polydomain to isotropic transition.

If the material is stretched in the polydomain state, the mesogens align themselves along the stretching direction and the material attains an anisotropic transparent monodomain state, becoming stiffer along the direction of stretch. The monodomain LCE becomes isotropic when heated and returns to polydomain upon cooling. Heating effectively 'erases' the mechanical deformation and resulting alignment.

This reset to the polydomain phase can be avoided with the help of photopolymerizable molecules. These molecules form chemical links between polymer chains when subjected to UV light. If the LCE containing photoinitiators is stretched and submitted to UV light, the formed chemical links lock the LCE in monodomain state and do not allow for a shift back to the polydomain phase [61]. During the monodomain to isotropic phase shift, LCE contracts in the direction of the mesogen orientation and expands along the transverse directions leading to a change in shape at constant volume, commonly called actuation.

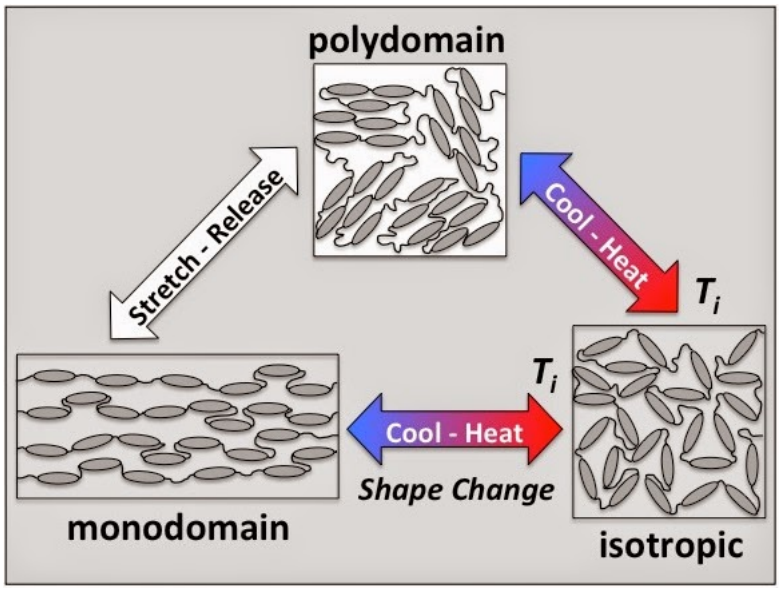

Figure 6: How mechanical and thermal stimuli influence three phases of LCEs: polydomain, monodomain, and isotropic [6]

Nematic-isotropic Transition Temperature (T_{NI})

LCEs exhibit various changes in physical properties due to the phase transition. For example, LCEs are capable of reversibly changing shape while transitioning between the nematic monodomain and the isotropic phase. To incorporate these physical property changes in practical applications, T_{NI} has to be tuned. For LCEs with disc shaped or rod shaped mesogens, T_{NI} can be manipulated by varying the structure of the mesogens and by changing the shape of the main polymer chain [62]. Moreover, the T_{NI} can also be systematically controlled through copolymerization including various non-mesogenic and mesogenic co-monomers [5].

Glass transition temperature (T_g)

T_g depends on the interactions between mesogens and the interactions between the polymer backbone and the mesogens [63]. The crosslinking density also influences T_g but the degree of influence varies with the degree of flexibility of the crosslinkers. For flexible crosslinkers and low crosslink densities, the crosslinker acts as a softening agent and Tg decreases with the increase in crosslinking density [5]. However , if the crosslinking density is increased further, the network becomes immobilized and T_g rises. For rigid crosslinkers, T_g keeps increasing with increasing crosslinker concentration. A higher crosslinking density can lead to the locking of liquid crystals in anisotropic glassy states creating duromers that exhibit various extraordinary properties [5].

1.2.3 Mechanical Behavior of LCE

LCEs exhibit both liquid crystalline behavior and rubber elasticity, which leads to extraordinary thermal and mechanical properties including high strain actuation and soft elasticity [55]

Phases and Anisotropy

Because the domain structure impacts the thermomechanical behavior, monodomain and polydomain LCEs have different mechanical properties [64]. In general, the Young's modulus of a monodomain LCE in the direction of the alignment is higher than the modulus of its polydomain equivalent. The Young's modulus and uniaxial thermal expansion of LCEs can also be tuned through the mesogen and crosslinking density [65].

Monodomain LCEs are anisotropic because of global mesogens orientation and exhibit reversible actuation. Polydomain LCEs are macroscopically isotropic. They are constituted of locally-oriented micro-domains, which globally reorient if subjected to a mechanical load [5]. This reorientation leads to the phenomenon of soft elasticity described in the next paragraph.

Soft elasticity

If a polydomain LCE is subjected to a uniaxial tensile load, the mesogens reorient themselves along the axis of loading to attain the monodomain phase [66, 67, 68, 69]. At low strain levels, the behavior is similar to that of an isotropic rubber. After exceeding loading threshold, the strain increases at constant stress, meaning almost no energy is required to cause deformation [66, 68]. Once the LCE has fully transitioned to the monodomain, the stress increases again with the increase in strain. The width of the soft elasticity plateau shortens as the temperature rises and the plateau fully disappears above the nematic-isotropic transition temperature (T_{NI}) [68]. Soft elasticity zone of the stress strain curve can be defined as the "deformation without resistance" region. This reorganization of mesogens and domains along the loading direction generates a viscous motion of the polymer chains, which facilitates the dissipation of mechanical energy [57].

Viscoelasticity

Studies show that LCEs exhibit interesting viscoelastic properties [67, 70]. LCEs can maintain a high loss factor throughout a wide range of loading frequencies [67], indicating they can dissipate a large amount of energy when subjected to a mechanical load of a wide range of frequencies. Following this idea, Traugutt et al. proposed LCE as a damping material against impacts [70].

Actuation

The most remarkable mechanical behavior of LCEs is their actuation properties. LCEs are capable of contracting in length when the temperature is raised over T_{NI} as they transition from monodomain to isotropic phase. Main chain LCEs have been reported to exhibit 400% actuation strain [71]. A strip of LCE is capable of lifting a weight that is almost 1500 times its own generating a stress of almost 300 KPa with a tensile stroke of approximately 50%, a specific work capacity of 50 J. kg^{-1}, and a work density of 96.9 kJ. m^{-3} [72]. These numbers closely resemble and sometimes exceed the behavior of human muscle tissues [71].

Fracture

The fracture energy of polydomain LCE can be increased by the polydomain to monodomain transition of the LCE near the crack tip [73]. This toughening mechanism is comparable to the toughening caused by phase-transition in ceramics or due to strain-induced crystallization in rubbers.

Mechanical behavior of printed LCEs

The mechanical properties of 4D printed LCEs have hardly been investigated in scientific studies. Printing speed affects the alignment of the mesogens [17], which, similarly to non-printed LCEs, is thought to impact the mechanical behavior. Various studies show that the angle of printing or the raster angle influences the mechanical properties of various 3D printed materials [74, 75]. Specimens printed from commonly-used materials, such as PLA and ABS, at different angles exhibit varying Young's Modulus, hardness, and ultimate tensile strength [74, 75].

1.3 4D Printing of LCE

LCEs can be combined with 3D printing technology to manufacture objects capable of large, reversible shape changes. In order to undergo a reversible shape change, LCEs need to be cross-linked in an aligned, monodomain state [71]. 3D printing has the potential to orient and align LCE mesogens directly while printing where-as traditional methods require an additional manufacturing step for the alignment of the mesogens [76].

1.3.1 3D printing techniques

Various approaches have been explored for 4D printing of LCEs in order to obtain a desirable orientated structure. Direct ink writing (DIW) has been the most commonly used and favored method for printing LCE actuators [77, 38]. As the viscous liquid crystal polymer (LCP) ink is pushed out of a small nozzle, shear thinning takes place resulting in the mesogens aligning along the printing direction. The alignment is then locked into an LCE monodomain state with the help of photocuring. Various 3D printing parameters like printing temperature, printing speed, nozzle to printing bed distance, etc. can influence the alignment of 4D printed LCEs [78, 17].

DLP can also be used for the 4D printing of liquid crystal elastomers. In DLP, LCE is printed via photocuring successive thin layers of photocurable thiol-acrylate liquid crystal resin [70]. More complex shapes can be achieved via DLP compared to DIW. However, the LCE is not oriented when printing via DLP. In this study, we have used the more common DIW method for the 4D printing of LCE, as it gave us more control on the setup and allowed for alignment during printing.

Although one of the main advantages of 4D printing is the lack of need for a second programming step, the printing and shape programming steps can still be decoupled which enables the manufacturing of a broad range of complex architecture capable of almost any type of arbitrary shape changes [76]. To attain this, LCE is printed into a reactive catalyst bath in the DIW method and is then programmed. The resulting LCE can switch between

the printed shape and the programmed shape as a function of temperature. This method cannot print structures with unsupported printed fibers [76].

1.3.2 LCP Ink

The success of LCE 4D printing relies largely on controlling the ink viscosity through temperature. The alignment of the mesogens has to be achieved at printing temperatures lower than T_{NI} to remain in the nematic phase but decreasing the temperature increases the ink viscosity, making it harder to push out through the small nozzle [14]. When the temperature is above T_{NI}, the ink becomes less viscous but the desired orientated structure can't be formed in the isotropic state.

The LCP ink is composed of mesogens, chain extenders, and photoinitiators. The length of the polymerization reaction is controlled to limit polymer chain length and viscosity [78, 79, 80]. Usually the printing temperature for LCE ranges from 50 to 105°C [81, 78, 80].

By using a solvent like acetone in the ink, the printing temperature can be brought down to 25-30°C. The T_{NI} for ink containing solvent is also lower, at around 75°C [79]. However, the solvent evaporates after printing and the printed object shrinks. The final shape of the object deviates from the printed shape. The post-printing shrinking is hard to predict and control, but the volume shrinkage due to solvent evaporation should be considered anyway to get the desired final shape [79].

In LCEs, temperature- dependent shape change is tied to processing conditions and the characteristics of the polymer network. Mesogen orientation is encoded when the material is printed in the nematic phase. Crosslinking locks the programmed molecular orientation in the LCE and stabilizes the nematic phase. In some LCP ink syntheses, variations in crosslinking density is used to introduce heterogeneity in the final elastomer network, which broadens the range of actuation temperatures [82, 72].

1.3.3 Performance

Although a new technological field, 4D printed LCEs have already been used in soft robots and dynamic functional architectures. LCEs printed via DIW at a high operating temperature could lift around 1000 times their own weight [78]. 4D printed aligned LCE filaments have been reported to undergo 40% reversible contraction along the printing direction [81]. By changing printing parameters during printing, site- specific shape morphing behavior can be introduced to 4D printed LCEs, rendering them functionally-graded [17]. Namely, nematic arrangements can be locally controlled by adjusting the printing speed and path to achieve complex deformations, such as locally programmed pop-up, self-assembly, snake-like curling, etc.

1.4 Complex Actuation and Soft Robotics

1.4.1 Definition of soft robots

Robots can be categorized as hard or soft based on the compliance of the material used to build them [83]. Soft robotics is a subspecialty of robotics that deals with soft materials characterized by a high compliance. Unlike conventional hard robots, soft robots can have

infinite degrees of freedom, continuous actuators, large material strains, and high dexterity [84]. Hard robots commonly have flexible joints connected by rigid links in order to perform repetitive, highly precise, pre-programmed movement patterns. Soft robots have continuous actuators that allow them to move in any direction in a 3D space and assume complex shapes at the expense of kinematic precision and ability to handle heavy payloads [83]. Soft robots possess a structure that is deformable continuously which is comparable to the actuation of muscles tissues and thus soft robots have a higher number of degrees of freedom in their movement pattern compared to the conventional hard robots [85]. The compliance and flexibility of soft robots make them harder to control.

1.4.2 Biomimetic

Soft robotics often draws inspiration from the movement pattern of biological organisms. Biological systems are usually constituted of soft and compliant materials that allow living organisms to exhibit reduced complexity and and maintain flexibility while interacting with their surrounding environment. Soft robots have the ability to bend and twist with a large radius of curvature that allows them to fit in and perform desired tasks in constricted spaces [86], adapt and change their shapes according to their surrounding environment [87], perform abrupt and agile movements that mimic bio entities [88]. Sometimes the softness of a robot can be limited to only certain parts of the robot. For example, a robotic arm made of rigid materials may have soft robotic grippers at the end of the arm to delicately grab objects of irregular shapes [89].

1.4.3 Artificial muscles

Soft robots need an actuation system in order to generate the necessary forces to carry out programmed movement commands. There are various ways to trigger the actuation in a soft robot. Actuation of smart materials can be triggered by stimulius such as electrostatic force, heat, pressure, etc. Dielectric Elastomers (DEs) are smart materials used in soft robotics as they responds to high voltage electric fields and change shape. These actuators are known to have high energy density and specific power, produce large strains and relatively high forces [90, 91]. DEs require a high voltage to trigger actuation, which becomes a problem in real life applications. The thermal actuation properties of shape memory polymers (SMPs) can also be used in soft robotics. Thermally activated SMP actuators can exhibit strains as large as 1000% [92]. However, the major drawbacks of using SMPs as actuators are that they have a slow response time and they generate a low amount of force [85]. Thermally activated shape memory alloys (SMAs) are also used as actuators even though they are rigid metals. The compliance of these actuators are just as high as soft materials as very thin pieces of wires or springs made of SMAs are used [93].

1.4.4 4D Printing in Soft Robotics

4D printing technology has a lot of potential applications in the field of soft robotics. The main feature in building 4D-printed soft robots is the use of 3D printed soft sensors and actuators [94]. For example, Kim et al. [95] additively manufactured an inflatable soft robot

with soft sensors and actuators that contained microfluidic sensors channels. When the channels are filled with a liquid conductor, they work like tactile sensors capable of determining the location and magnitude of external forces [95]. The 4D-printed soft robot inflates and deflates in accordance with the forces measured by the 4D-printed sensory system.

1.4.5 Soft LCE Robots

Soft robots made of LCE actuators have been the focus of various research studies. For example, light-responsive LCEs have been used in soft robots mimicking the locomotion of an inchworm [96] and of a caterpillar [97]. Structured monochromatic light can be used to trigger a micro-scale local expansion in photo-responsive LCE microfibers and the local deformation can lead to various complex biomimetic movement patterns [98]. Even though the developments in the use of LCE in the field of soft robotics is promising, LCEs have a few problems that need addressing before they can be widely used to manufacture soft robots. The actuation time in LCEs ranges from seconds to several hours which is long for soft robotics applications [99, 100]. Moreover, most soft robots made of LCE have a limited range of motion and actuate in only one or two planes. Various complex movement patterns like combined translation and rotation cannot be achieved with LCE soft robots [48].

1.4.6 Soft 4D-printed LCE robots

Recently, 4D printing technology has introduced the encoding of molecular order and local material programming to additively manufactured LCE soft robots that can lead to complex actuating shapes [48]. Roach et. al. [79] used 4D printed LCEs to manufacture a multi-material active hinge. Conductive wires were sandwiched between a 3d-printed, heat activated LCE strip and an elastomer layer. As the wire heated up the LCE strip, it contracted in length and the large strain gradient between the contracting LCE strip and the elastomer layer resulted in bending of the hinge. Using the same principles, they manufactured a soft-robotic gripper consisting of four 3D-printed LCE hinges capable of gripping and raising a ping pong ball [79].

1.5 Motivation

4D printing is a recent technology with a room for improvement. Using LCEs in 4D printing is an even more recent concept with untapped potential in terms of applications. In traditional LCEs, the synthesis methods require a second step for proper mesogen orientation to achieve actuation. In 3D printing, the LCP ink can be deposited directly aligned on the printing bed. Exploiting this perk is the fundamental motivation behind combining LCE with additive manufacturing technology to manufacture 4D printed objects.

Mesogen alignment strongly correlates with LCE actuation [17]. Hence, the mesogen orientation and the actuation of the 4D printed LCE is regulated by a number of printing parameters, such as printing temperature, printing speed, nozzle to printing bed distance, printing angle, etc. Finding the best actuation conditions is another motivation for this study. Shear thinning of the ink has to take place in the nozzle in order for the mesogens to be deposited in an aligned manner on the printing bed. In the same way, optimum printing

speed and, nozzle-to-bed distance should be set to ensure the best actuation. There remains a number of unknowns regarding the influence of printing parameters on the resulting LCE actuator.

LCEs exhibit a unique thermomechanical viscoelastic behavior. It has been shown that the mechanical properties of printed materials differ from their bulk, non-printed, counterparts. The mechanical properties of 4D printed LCEs have been little explored as most studies focus on actuation. In addition, it is expected that printing parameters influence the viscoelastic mechanical behavior of the resulting material.

Recent studies show that various complex actuating shapes can be achieved via 4D printing [81, 79, 17]. Since a mathematical model to predict the change in shape from local orientation in LCE is still eluding researchers, the design of complex actuators remains driven by trials and errors.

4D printed LCEs haves been used in soft robotics within a limited scope. Unlike traditional robotics, the goal of soft robotics is for all components to remain soft, meaning no motor or electro-mechanical signal. As 4D printed LCEs exhibit actuation properties that bypass the need for incorporation of an external electro-mechanical system, they are ideal for soft robotics applications. As 4D printing remains in its infancy, the design of LCE soft robots involving locomotion or complex motions remains limited to a few examples.

LCEs are biocompatible materials. LCEs first came into the spotlight when studies showed that they had the potential to imitate real muscle movement patterns [101, 100]. We are motivated to explore different potential applications of 4D printed LCE ranging from dynamic architecture to customized prosthetics. We have tried to explore different avenues of practical application for this relatively new field of research.

1.6 Objectives

Additive manufacturing is a complex process in itself but additive manufacturing with the prospect of post-manufacturing shape change requires even more precision and parameter optimization. One of our primary objectives is to determine the optimal parameters for LCE 4D printing. We will focus on printing speed, which has to be fast enough to promote shear thinning and the alignment of mesogens but slow enough to avoid printing broken lines, and on raster angle, which allows for more complex actuations. Apart from actuation, 4D printed LCEs need to exhibit sound thermo-mechanical properties. The goal is to define the printing parameters optimized for actuation and for mechanical properties. We also aim at finding how the thermomechanical viscoelastic properties vary with printing speed and angle. We are also interested in determining how the mechanical properties of 4D printed LCEs differ from the properties of bulk LCEs.

4D printing has opened the door for highly complex post-manufacturing shape-morphing behavior of smart materials. 4D printed LCEs have the potential to exhibit complex actuation. One of our goals is to attain controlled, complex actuation by fine-tuning printing speed, raster angle, and material programming. Finally, we want to explore the potential application of 4D printed LCEs in soft robotics and manufacture dynamic functional structures.

CHAPTER II

The Influence of Printing Speed and Raster Angle on the Actuation of 4D Printed LCE

2.1 Materials and Method

2.1.1 Preparation of the LCE Ink

The synthesis procedure uses a catalyst-free Michael addition reaction specifically developed to prepare solvent-free LCE [78]. Equal molar quantities of mesogens RM82 (1,4-Bis-[4-(6-acryloyloxyhexyloxy) benzoyloxy]-2-methylbenzene, from Wilshire Technologies, Princeton, NJ, USA) and polymer spacers n-butylamine (Sigma-Aldrich, Saint Louis, MO, USA) were mixed in a beaker. The photoinitiator Irgacure 369 (Sigma-Aldrich, Saint Louis, MO, USA) was added at a ratio of 2%wt of the mixture. The mixture was placed in an oven at 110°C

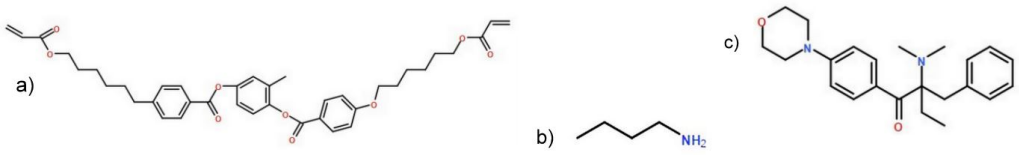

Figure 7: a) Mesogen molecule (RM82) b) Polymer spacer (n-Butylamine) c) Photoinitiator

(above the nematic-isotropic transition temperature of the resulting LCE) until a liquid solution is obtained. The solution was mixed for several minutes with a vortex mixer (Fisher Vortex Genie 2) and poured in a syringe, wrapped in a light-shielding aluminum foil. The solution oligomerized in the oven at 110°C for 18 hours. Finally, the syringe was submerged in an ice water bath for 5 minutes to stop the reaction. This method prepares a liquid crystal polymer ink. As the ink crosslinks under UV light during printing, a liquid crystal elastomer is formed.

2.1.2 3D Printing and Specimen Preparation

A commercial printer (Ultimaker 2.0) has been customized to perform direct ink writing. A piston extrusion system to push the LCE ink out of a 9.59mm-diameter syringe is controlled by a servomotor. A heating cartridge allows to control the temperature of the ink to be printed. A heat sleeve has been installed to maintain uniform temperature profile of the ink throughout the feeding system. The syringe is loaded in the printer and heated to 50°C for 10 minutes before printing. The diameter of the printing needle was 0.25 mm. The

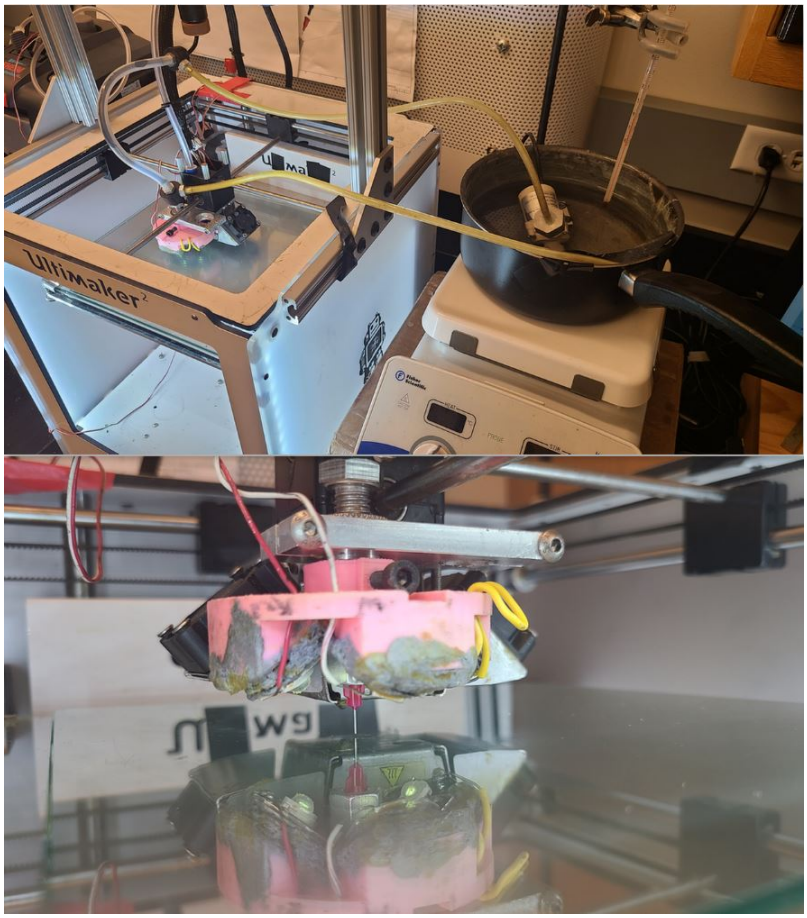

Figure 8: The 3D printing setup

displacement and speed of the needle were controlled by two servomotors, implementing the sequences programmed in a G-code defining the print. Specimens were printed on clean glass plates. The layer height was kept at 0.1 mm for all specimens. Unless stated otherwise, the airgap between adjacent lines was set at 0. A UV LED system at a 390nm wavelength was built around the needle for instantaneous curing while printing Specimens are placed under a static UV lamp (Intensity: 22 mW/cm^2) with a wavelength of 365 nm for 15 minutes after printing to ensure full curing.

Single-layer specimens of dimensions 20 mm×3mm were printed at printing speeds of 0.5, 3, 6, 8, 10, and 12 mm/s and the specimens were subjected to DMA tests, tensile tests and actuation tests. Single-layer specimens were also printed at raster angles of 0°, 22.5°, 45°, 67.5°, 90° and a speed of 10 mm/s and the specimens were subjected to the same tests. In order to compare various properties of 4D printed LCE with bulk LCE, non-printed specimens were prepared. Those specimens were prepared by manually pushing LCE ink out of a syringe (barrel diameter of 9.59 mm and nozzle diameter of 1.75 mm) in a dumbbell shaped die. The dye containing the LCE ink was then put under a static UV lamp (Intensity: 22 mW/cm^2) for 30 minutes before peeling them out of the die.

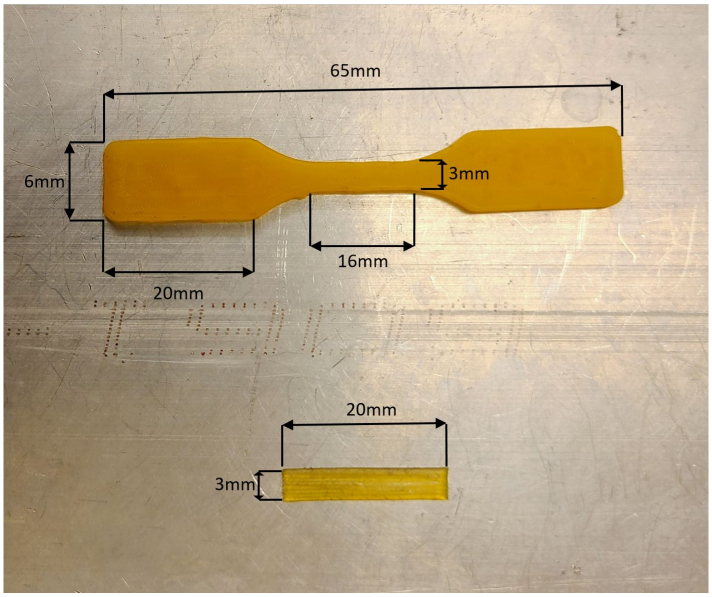

Figure 9: The specimens and their dimensions

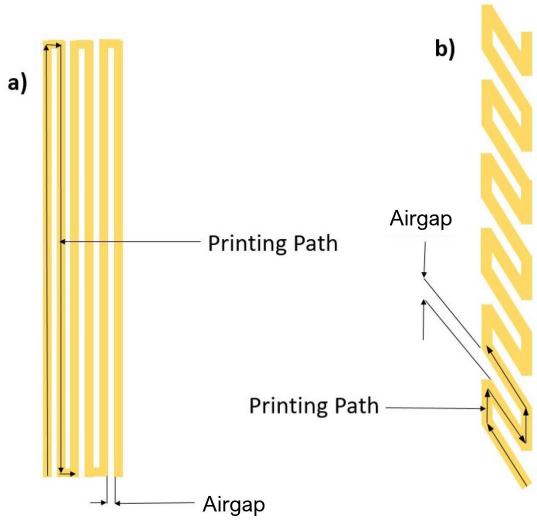

Figure 10: Printing path for rectangular specimens printed at a) 0° angle and b) 45° angle

2.1.3 Characterization

Polarized Optical Microscopy

The birefringence linked to the orientation of the liquid crystals in the printed specimens was observed with a polarized light microscope (Olympus BX53M) at room temperature. The samples were placed between two polarizers orthogonal to each other (cross-polarized system). The observation bed was rotated at various angles to observe the specimens at various orientations with respect to the polarizers. Focusing was performed manually by adjusting the proximity between the movable observation bed and the observer lens. 10x magnification was used without any birefringence amplifier in order to observe the specimens.

Actuation strain

To measure the actuation, that is the change in shape around the nematic-isotropic transition of the LCE, the specimens were placed on a heater plate (Fisherbrand Isotemp Hotplate Stirrer) coated with silicon oil. The plate temperature was maintained at 95°C. The change in shape was recorded with a video camera and the actuation strain was quantified by processing the images in MATLAB (The Mathworks, Natick, MA, USA). 10 measurements of the actuation strain and the radius of curvature were taken respectively for specimens printed at different speeds and angles. The mean and standard deviation of those measurements were plotted using Matlab.

2.2 Results and Discussion

2.2.1 Mesogen Alignment

Controlled molecular orientation was generated in the specimens printed at different speeds and different angles due to DIW printing. When the orientation of the printed fibers were

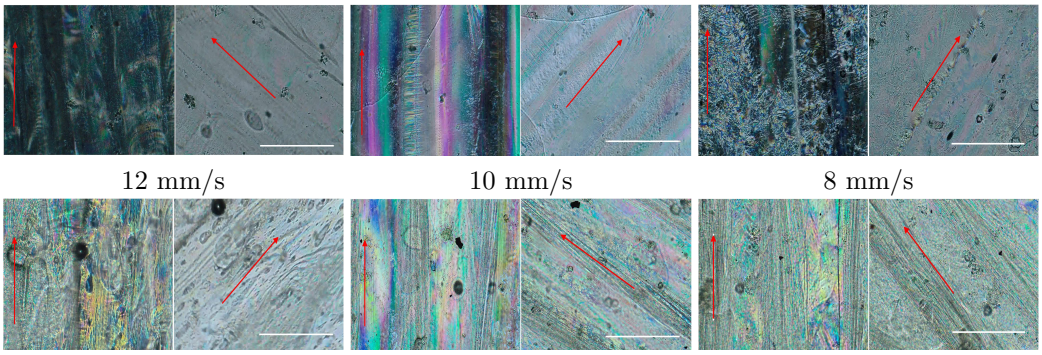

Figure 11: Polarized light microscope images showing birefringence of specimens printed at different speeds at 0° (dark) and 45° (bright) to the polarizer. The red arrows indicate the direction of the printed filaments. White scale bar: 250 μm

perpendicular or parallel to the polarizers, the specimens looked dark but when the fibers were at a 45° angle with the polarizers, the specimens looked bright (Figures 11 and 12). The shift in brightness was barely discernible at lower printing speeds but highly prominent at higher printing speeds. The shift in brightness did not vary significantly with the change in printing angles. These results are consistent with previous studies [81, 14, 79]. During DIW printing of LCE, the mesogens get aligned along the printing direction as the ink is pushed out of the nozzle under high pressure and shear thinning [78]. The alignment of mesogens is necessary for the LCE to reach the monodomain phase. In the monodomain phase, LCEs exhibit briefringence, i.e. optical anisotropy. When the printing direction of the specimen is parallel or perpendicular to the polarizers, polarized light can not pass through and so the specimens look dark. But if the orientation of the printing direction is changed to 45° with respect to either of the two polarizers, polarized light can pass and the specimen looks bright. This phenomenon can not be observed in case of polydomain or isotropic LCE as they exhibit optical isotropy. So polydomain and isotropic LCEs do not change brightness at different

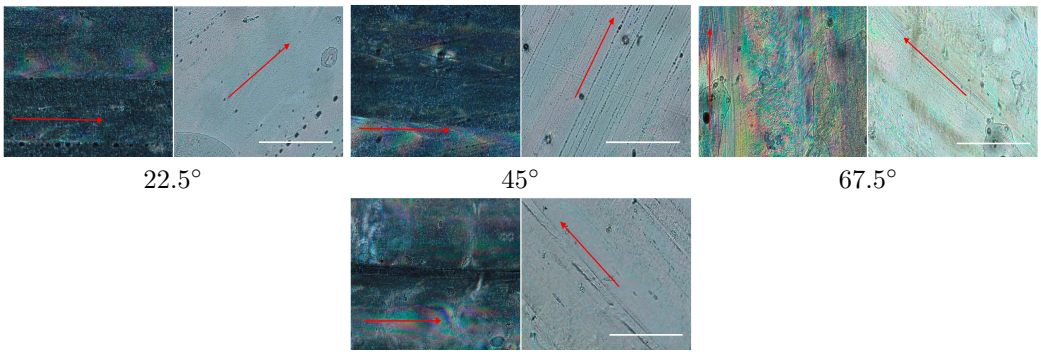

Figure 12: Polarized light microscope images showing birefringence of specimens printed at different angles at 0° (dark) and 45° (bright) to the polarizer. The red arrows indicate the direction of the printed filaments. White scale bar: 250 μms

angular orientations of the printing direction with respect to the polarizers. Consequently, the change of brightness of the specimens in polarized microscopy is an indication of proper alignment of mesogens along the printing direction. Polarized light microscopy does not measure the exact degree of alignment of mesogens but the relative degree of alignment of mesogens of different specimens can be inferred from those images. Figure 11 shows that the change in brightness is higher for specimens printed at higher printing speeds which seems to indicate that the degree of order of the mesogens is higher. In case of specimens printed at different angles, all the specimens were printed at the same 10 mm/s speed and the shifts in brightness were identical. So the degree of alignment of the mesogens seems to depend on the printing speed but not on the printing angle.

2.2.2 Actuation Tests

Actuation Strain for Specimens Printed at Different Speeds

The specimens actuated and exhibited both longitudinal and lateral strain as the temperature was raised above the T_{NI} (figure 13). Both lateral and longitudinal strains increased with the rise in printing speed. The specimens contracted longitudinally and expanded laterally and the curves show the absolute values of those strains. The specimen with 0 mm/s printing speed represents the non-printed bulk LCE specimen. Actuation strain initially tends to increase with the rise in printing speed but after 10 mm/s, printing speed doesn't significantly affect the actuation strain. These results are consistent with previous studies [17, 78]. The actuation happens due to the transition of LCE from the aligned monodomain phase to the non-aligned isotropic phase. Studies have showed that a higher degree of alignment of the mesogens corresponds to higher actuation strains [102, 78]. This phenomenon can be explained by the two forces at play during printing—the shearing force and the stretching force [17, 103]. The shearing force causes the shear thinning of the LCE ink as it is squeezed out of the fine needle. When the material is deposited on the printing bed, the stretching force or tensile force arises between the tip of the nozzle and the printing bed. The alignment of the mesogens depends on these two forces and these forces depend upon the printing speed and the printing temperature [78]. With the rise in printing speed, the stretching force increases

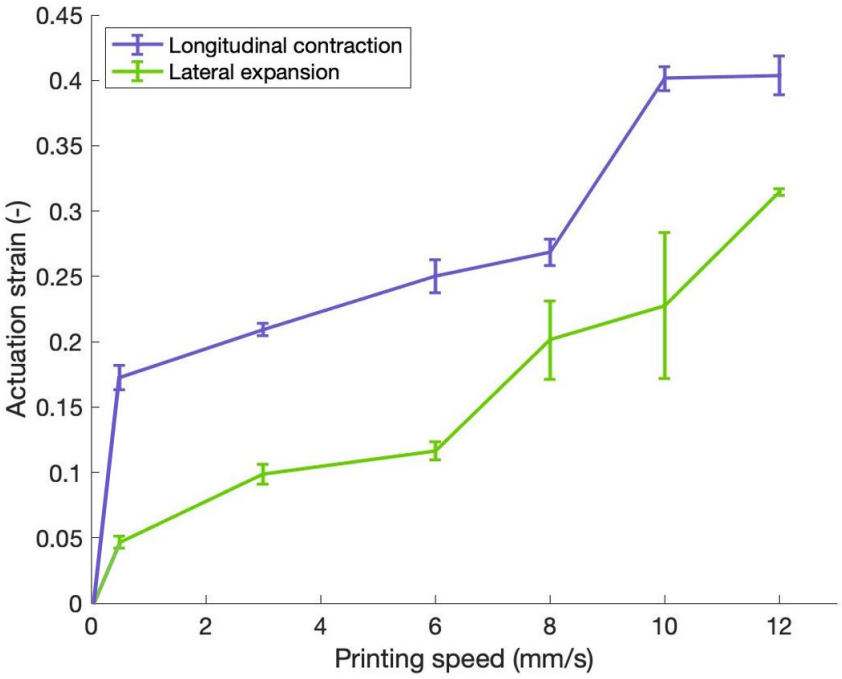

Figure 13: Longitudinal and lateral strain of specimens printed at different angles. The error bars signify 1 standard deviation

and the mesogens tend to be more aligned along the printing direction which in turn leads to a higher actuation strain. If we assume the LCE to be a linearly elastic material, we can explain how printing speed affects the alignment of mesogens and the actuation of LCE with the following equation [17]:

$$\varepsilon = \varepsilon_0 + vt$$

In this equation, ε denotes strain after depositing the ink, ε_0 is the initial strain after extrusion, t is the contact duration of the extruded LCE and the substrate and v is the printing speed. From the equation, it can be observed that higher printing speeds result in higher embedded strains. Higher the embedded strain leads to better alignment of the mesogens which in turn generates higher actuation strain. The non-printed bulk LCE was in polydomain phase with no alignment of mesogens and so the bulk LCE specimen exhibited no lateral or longitudinal actuation at all.

Actuation Strain for Specimens Printed at Different Angles

While specimens printed at 0° printing angle exhibit longitudinal and lateral actuation strain, specimens printed at different angles tend to bend and form a circular shape (Figure 14). The

Figure 14: Actuation of specimens printed at different angles. Black scale bar: 5mm

radius of curvature of specimens printed at different angles are shown in figure 15. Radius of

curvature decreases with the increase in printing angle. The specimen printed at 22.5° angle forms a semi-circular shape where as the The specimen printed at 90° angle coils into a small circle. When specimens printed at any angle other than 0° are heated, the fibers contract

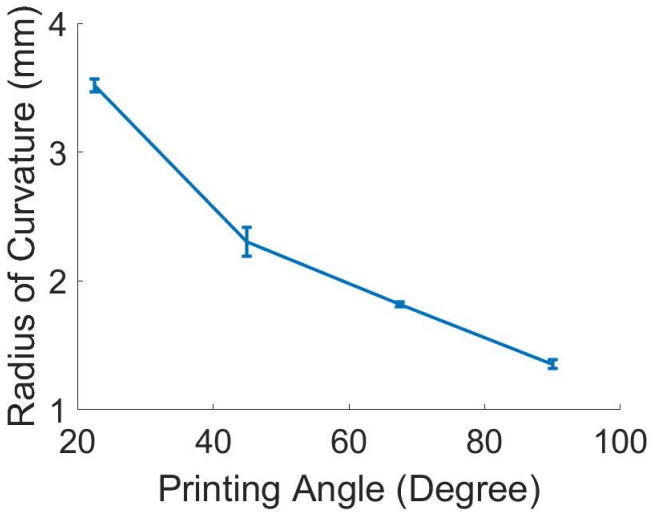

Figure 15: Radius of curvature of specimens printed at different angles

along the printing direction. This generates a bending force that bends the specimens into circular shape.

CHAPTER III

The Influence of Printing Speed and Raster Angle on the Mechanical Properties of 4D Printed LCEs

3.1 Materials and Method

3.1.1 Characterization

To find the mechanical properties of specimens printed at different speeds and angles, Dynamic Mechanical Analysis (DMA) and tensile tests were performed. The specimens tests were prepared exactly as described in chapter 2. The dimensions of the specimens were also as stated before.

Dynamic Mechanical Analysis

The Dynamic Mechanical Analysis tests and tensile tests were performed on the RSA-G2 analyzer (TA instrument). An oscillation test with 6 different frequencies (5Hz, 10Hz, 20Hz 30Hz, 40Hz, 50Hz) was performed on all the specimens. Data acquisition mode was transient with 128 points per cycle. The strain amplitude was .1%. The data obtained was processed in Matlab to find the storage modulus, the loss modulus and the loss factor ($\tan\delta$ where δ is the phase angle) of the specimens.

For the tensile test, the materials were tested at .1%/s strain rate at room temperature. The test was carried out until failure. The data was analyzed in Matlab to find out the Young's Modulus and the stress-strain curves of the specimens printed at different speeds and angles. The Young's modulus is determined as the slope of the stress-strain curve at low strains, below 2%.

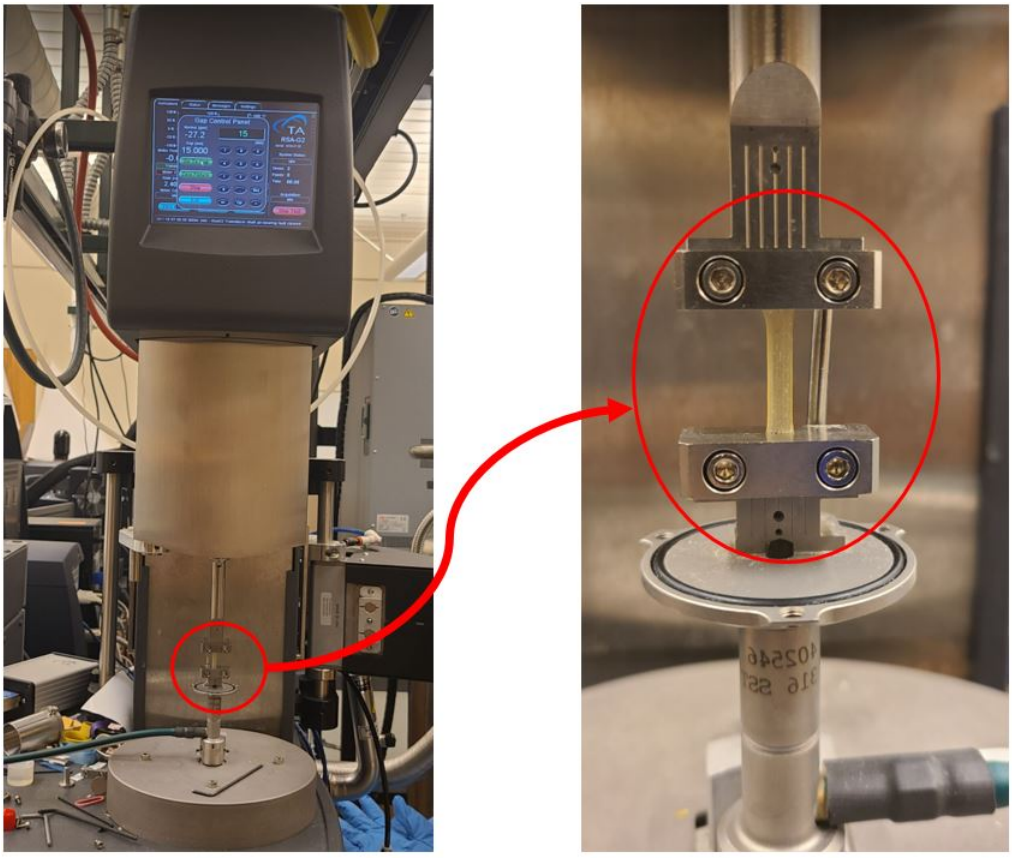

Figure 16: Experimental setup for the DMA and tensile test

3.2 Results and Discussion

3.2.1 Young's modulus

Influence of Printing Speed

The stress-strain curves for specimens printed at different speeds are shown in figure 17. Here, the 0 mm/s printing speed represents a non-printed bulk LCE specimen. The Young's modulus first increases and then decreases with the increase in printing speed. The bulk LCE specimen has the lowest Young's modulus. 4D printed LCE specimens printed at various speeds have a significantly higher Young's modulus compared to the non-printed bulk LCE. The main difference between the bulk LCE and the 4D printed LCE is that the 4D printed LCE has aligned mesogens. We have discussed in the previous chapter how the alignment of mesogens affects the actuation and it can be observed here that the alignment of mesogens affects LCEs' mechanical properties as well. Even though the alignment of mesogens is better at higher printing speeds, the Young's modulus drops at printing speeds over 8mm/s. The rise and drop in Young's modulus with the increase in printing speed is consistent with the findings in previous studies [17]. At higher printing speeds, the alignment of mesogens is better. The better alignment of mesogens leads to a higher stiffness and Young's modulus. The initial rise in Young's modulus can also be explained with the help of the core-shell structure theory developed by Gantenbein et al. [104]. According to this theory, the extruded

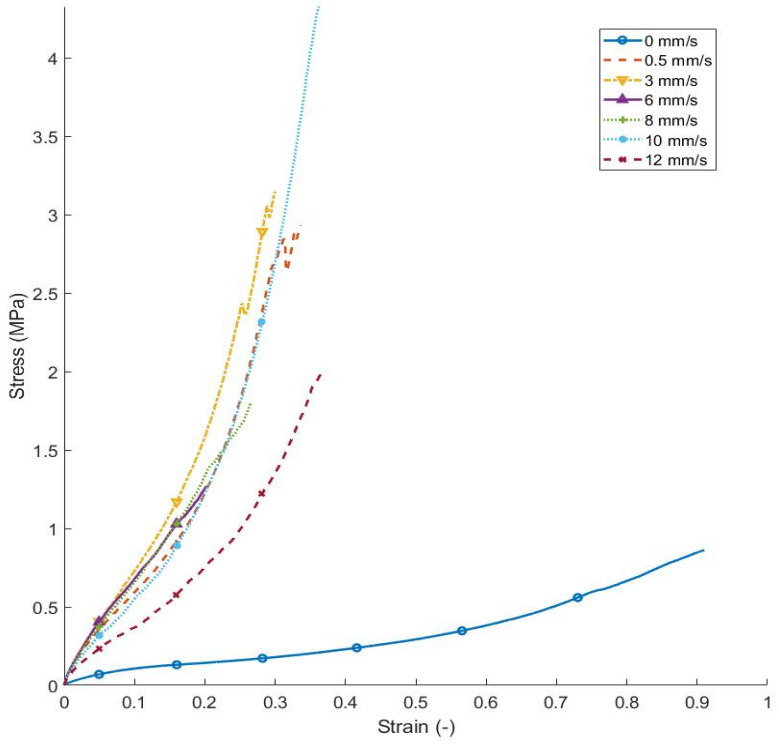

Figure 17: Stress-strain curves for specimens printed at different speeds. The 0 mm/s specimen represents the non-printed, bulk LCE specimen

filament consists of an aligned shell encompassing a less aligned core. The analytical model below shows that shell formation can be traced to the cooling mechanism of the extruded material [104, 17]:

$$S(t) = S_0 e^{-t/\tau}$$
$$E = \phi_{shell} E_{shell} + \phi_{core} E_{core} \approx \phi_{shell} E_{shell}$$

Here,

S = Degree of orientation
S_0 = the initial flow-induced orientation
t = the cooling timescale
τ = the relaxation time of the LCE domains
E = Elastic modulus of the final product
E_{shell} = Elastic modulus of fully aligned LCE
ϕ_{shell} = the volume fraction of aligned material across the filament

Gantenbein et. al. showed that rapid cooling at the extruded filament surface results in the solidification of the nematic order and slower cooling leads to the reorientation of the polymer chain [104]. At higher printing speeds, rapid cooling will take place and the cooling

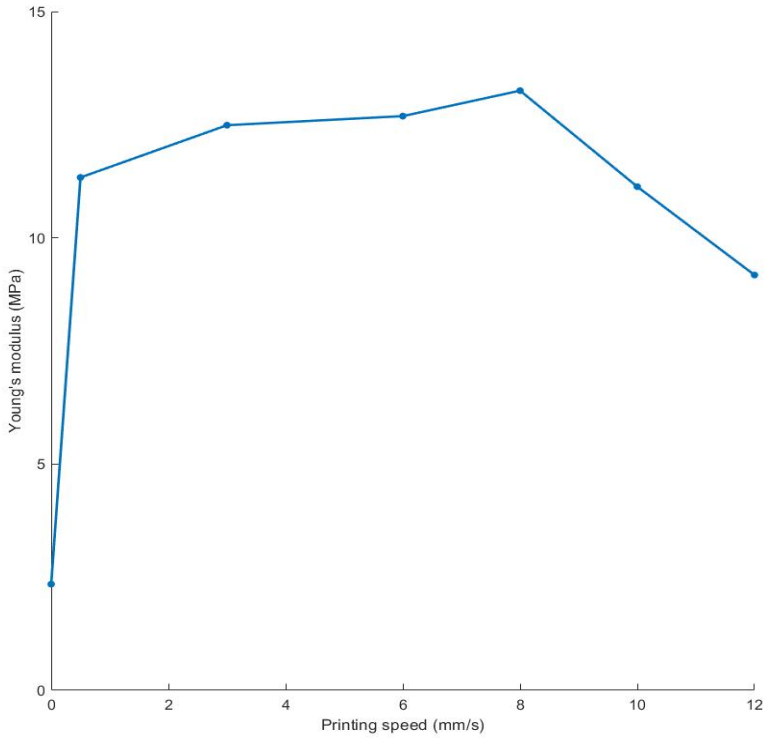

Figure 18: Young's modulus for specimens printed at different speeds. The 0 mm/s specimen represents the non-printed, bulk LCE specimen

time (t) will be shorter and so the oriented shell layer will be thicker [17]. A thicker, more oriented shell will lead to higher mechanical strength (E). This is how a higher printing speed contributes to a higher Young's modulus. That is also why the non-printed Bulk LCE (printing speed 0 mm/s) has the a very low Young's modulus compared to 4D-printed LCE. But above the printing speed of 8 mm/s, Young's modulus decreases. This can be attributed to the poor quality of printing at higher printing speeds. Previous studies have shown that when the printing speed increases above a threshold, the viscous ink cannot strongly attach to the printing bed due to the limited time of contact [17]. This leads to an uneven deposition of the filament as well as rough filament surface. In this study, we assume such threshold is reached above 8 mm/s, which explains the decrease in mechanical performance at higher speeds, independently of the degree of alignment of the mesogens.

Influence of Raster Angle

As shown in figure 19, the slope of the stress vs strain curves for specimens printed at different angles decreases with the increase in printing angle. The drop in Young's modulus is more significant at printing angles between 0° and 45° at printing angles higher than 45° the stress-strain curves are clustered together. Figure 20 shows that the Young's moduli are higher at lower printing angles. These results are consistent with the findings of previous studies on the tensile properties of 3D printed materials printed at different angles [75, 74,

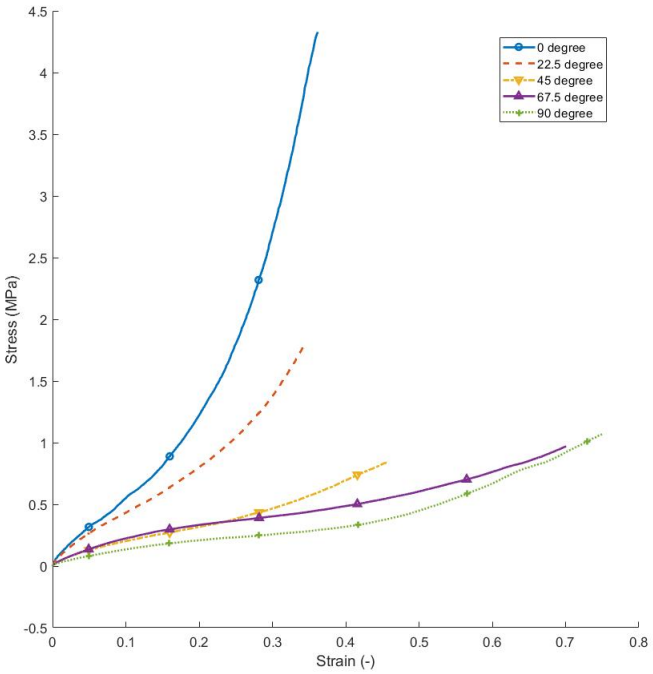

Figure 19: Stress-strain curves for specimens printed at different angles

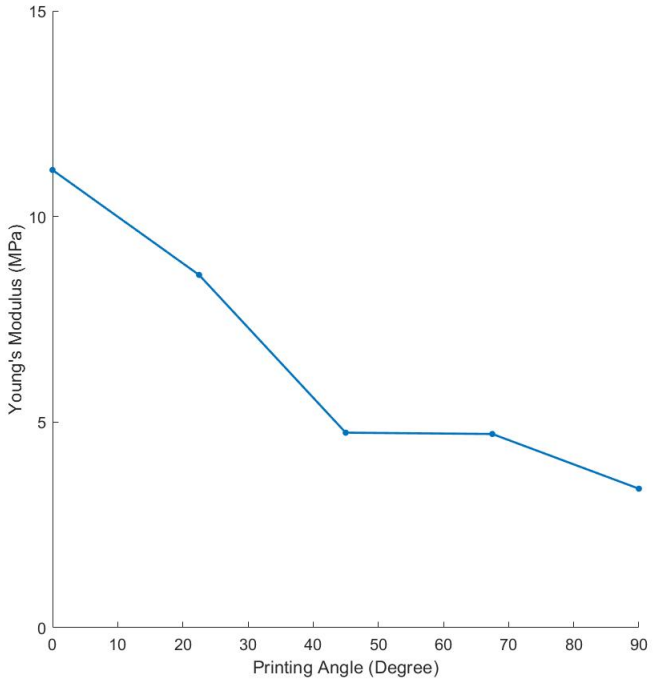

Figure 20: Young's Modulus of specimens printed at different angles

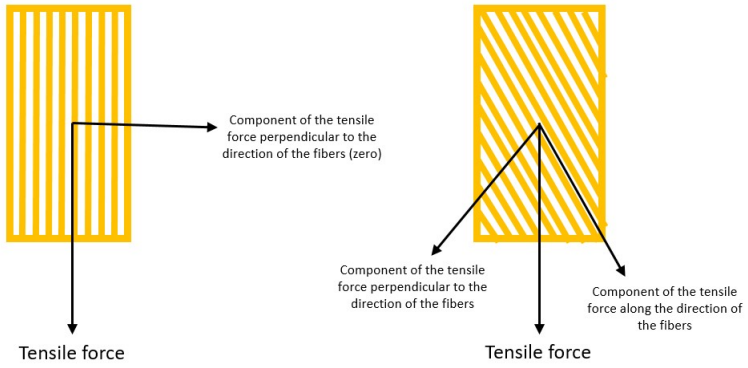

Figure 21: Direction and components of the tensile force on a) specimens printed at 0° raster angle and b) specimens printed at 45° raster angle

105, 106].The elastic modulus also decreases with the increase in printing angle in case of 3D printed materials like Acrylonitrile Butadiene Styrene (ABS)[75], Polycarbonate (PC)[74] and Polypropylene (PP)[106]. The printed specimens are the strongest along the printing direction. So for lower angles between the tensile axis and the direction of the fibers in the material, the Young's Modulus is higher. The fibers are the strongest along the longitudinal direction but as the adhesion between two side by side fibers is not as strong, the specimens are not as strong in the direction orthogonal to the printing direction. When the specimen is printed at 0° raster angle, the direction of the tensile force is aligned with the direction of the fibers and there is no component of the axial force acting perpendicular to the fibers (Figure 21). But at any printing angle other than 0°, there exists a component of the tensile force along the perpendicular direction of the fibers. This force breaks the bonds between two adjacent fibers. This is why specimens printed at any angle other than 0° did not exhibit the same level stiffness.

3.2.2 Viscoelastic Properties

Influence of Printing Speed

The DMA test results are shown in Figure 22 and 23. The 0 mm/s printing speed represents a non-printed bulk LCE specimen. Both the moduli increased with the rise in frequency. Apart from the non-linear behavior at 40 Hz frequency, the general trend of the storage and loss modulus was to first rise and then drop with the increase in printing speed. The storage and loss moduli also increased with the increase in frequency for all printing speeds. Figures 22 and 23 also show that the viscoelastic response for the 4D-printed LCE was quite different from the non-printed bulk LCE. The storage and loss modulus for the bulk LCE specimen were lower at all frequencies. This indicates that 4D printed LCE is stiffer and can dissipate more energy than bulk LCE. The main micro-structural difference between the printed and bulk specimens was that the printed specimens contain more aligned mesogens and probably an aligned polymer main chain. Indeed the printed LCE specimens were mostly in the monodomain phase while the bulk LCE was in the polydomain phase. Similarly, Linares

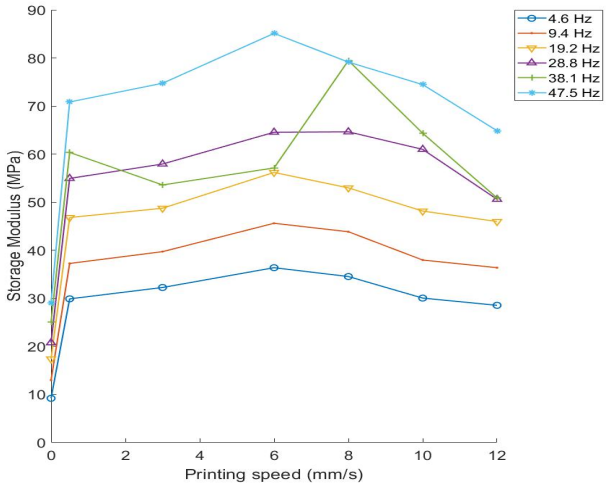

Figure 22: Storage modulus for different printing speeds at different frequencies

et al. showed that the alignment of mesogens have a significant impact on the viscoelastic behavior of LCE and monodomain LCEs exhibit a higher storage and loss modulus compared to polydomain [107]. So the 4D printed LCE specimens had a higher loss and storage modulus due to a higher degree of alignment of the main chain and mesogens compared to the bulk LCE specimen.

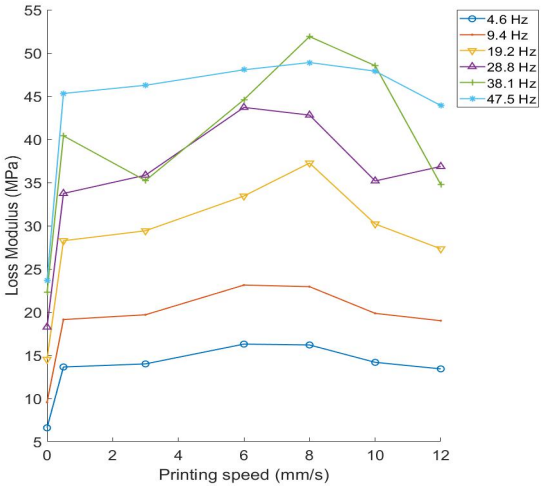

Figure 23: Loss modulus for different printing speeds at different frequencies

From the actuation tests described in Chapter 2, it was observed that the specimens printed at lower speeds had a lower actuation strain which was an indication of lower degrees of alignment of mesogens at those printing speeds. Even at lower printing speeds, the specimens were aligned enough to exhibit almost twice as high loss and storage modulus compared to the bulk LCE. This shows that the 3D printing process significantly alters the viscoelastic behavior of LCE. The DMA tests also prove that 4D printed LCE is indeed viscoelastic exhibiting both viscous and elastic behavior.

Influence of Raster Angle

From figure 24 and 25 it can be observed that both the loss modulus and storage modulus dropped with the increase in printing angle. Both storage and loss modulus increased with the increase in frequency for all printing angles. As observed in the case of the specimens printed at different speeds, there was some non-linear behavior at 40 Hz frequency for specimens printed at different angles.

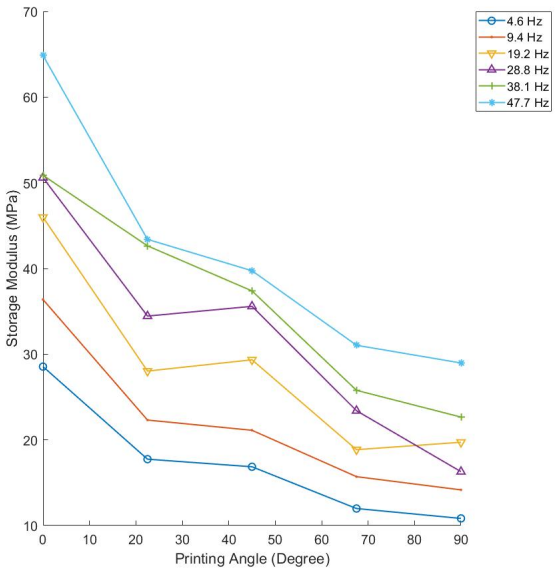

Figure 24: Storage modulus according to printing angles at different frequencies

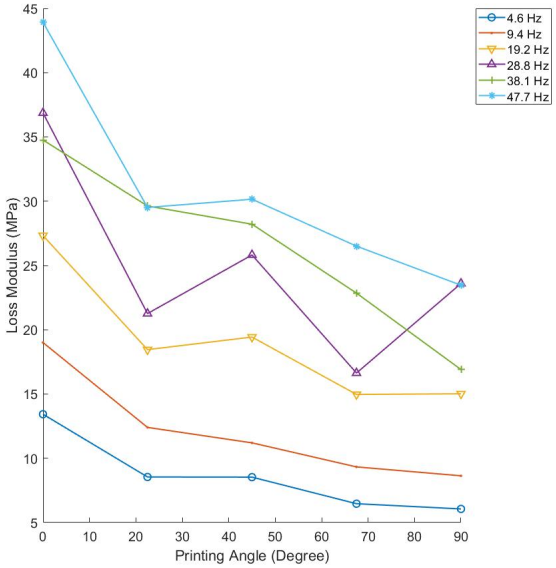

Figure 25: Loss modulus according to printing angles at different frequencies

The decrease in loss and storage modulus indicates that the specimens become less elastic and dissipate less energy as the printing angle rises. The tensile tests showed that the elastic modulus decreased with the increase in printing angle which is consistent with the findings in the DMA test. For the specimen printed at 0°, the direction of the imposed sinusoidal stress during the DMA test was along the direction of the printed fibers. The specimens are the strongest along the direction of the fibers. At higher printing angles, the direction of the stress was at an angle with the direction of the fibers. That is why the specimen printed at 0° have the highest storage modulus and specimens printed at higher printing angles have a lower storage modulus. At higher printing angles, the energy dissipation between filaments decrease and so the loss modulus decreases.

CHAPTER IV

Application to Soft Robotics: Actuation Programmed by Layer Orientation

4.1 4D Printed LCE Helices

Helical shapes can be attained from 2D rectangular LCE strips by varying the printing path and printing conditions. This is one example of 2D-to-3D shape-morphing attainable via 4D printing. We have combined the effects of printing speed and printing angle on actuation to prepare helices that have varied pitch lengths.

4.1.1 Specimen Printing and Actuation Method

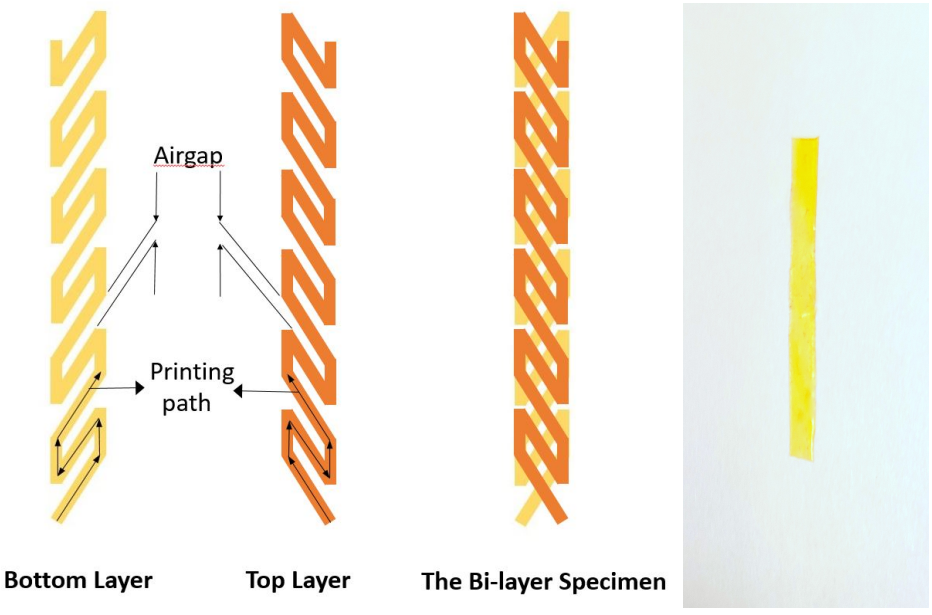

a) b)

Figure 26: a)Printing path of the helix and b) the LCE helix at undeformed, neutral state

The LCE ink has been prepared as described in chapter 2. The flat rectangular LCE specimens consist of two layers. Both layers have the same dimensions, 20 mm in length and 3 mm in width. To attain the helical shape upon heating, the layers need to be printed at an angle other than 0° or 90°. We printed the bottom layer at 22.5°, 45° and 67.5° angles and the top layers were printed at a supplementary angle to the bottom layer (Figure 26). Both

layers were printed at the same speed. We manufactured 9 helices, 3 helices for each angle at 3 speeds (3, 6, 10 mm/s). The airgap was 0 mm and printing temperature was 50°C.

The pitch of a helix is the height of one complete helix turn, measured parallel to the axis of the helix. If a helix has a small pitch that means the turns in the helix are closely packed. In this study, we measured the pitch of the helices to find out how printing angle and printing speed affect the pitch of 4D-printed LCE helices.

To measure the actuation, the helices were heated on a heater plate at 95°C. Photos were taken as the flat rectangular LCE strips assumed helical shapes. The images were then processed via Matlab to find the pitch of the helices. The pitch was measured 5 times for each helix and the mean and the standard deviation of the measurements were plotted via Matlab.

4.1.2 Results and Discussion

The formation of helices printed at different angles and speeds are shown in figure 27. The pitch of the helices decreases as the printing speed and angle increase. Lower pitch length means more compactness of the helices or more turns per unit length. So with the rise in printing angle and printing speed, the helices become more compact and the turns in the helices come closer together. But if the printing angle nears 90°, helices do not form. The relative decrease in pitch from 3 mm/s to 10 mm/s speed for the helices printed at 22.5° is 29.26% but for helices printed at 67.5°, the relative decrease in pitch is 11.22%. This shows that the effect of printing speed on the pitch of the helices become less influential at higher printing angles.

The helices consist of two layers printed at supplementary angles. When the specimens are heated, the two layers bend in the opposing directions creating a twisting motion in the structure which leads to the formation of the helical shapes. As higher printing angles lead to a higher degree of contraction during actuation, the helices twist more and create more turns at higher printing angles. Similarly, higher printing speeds contribute to a higher degree of actuation and the helices have more turns when printed at higher speeds.

4D printed helicoids have been manufactured in previous studies as well. Gladman et. al. prepared a bio-inspired Dendrobium helix with hydrogels [1]. Hydrogels were printed at supplementary angles in 2 layers and when the structure was submerged in water, it assumed a helicoid shape. Same printing principles with different materials were used in this study as well in order to get the helical shape but we further investigated how printing parameters can influence the pitch of 4D-printed helices.

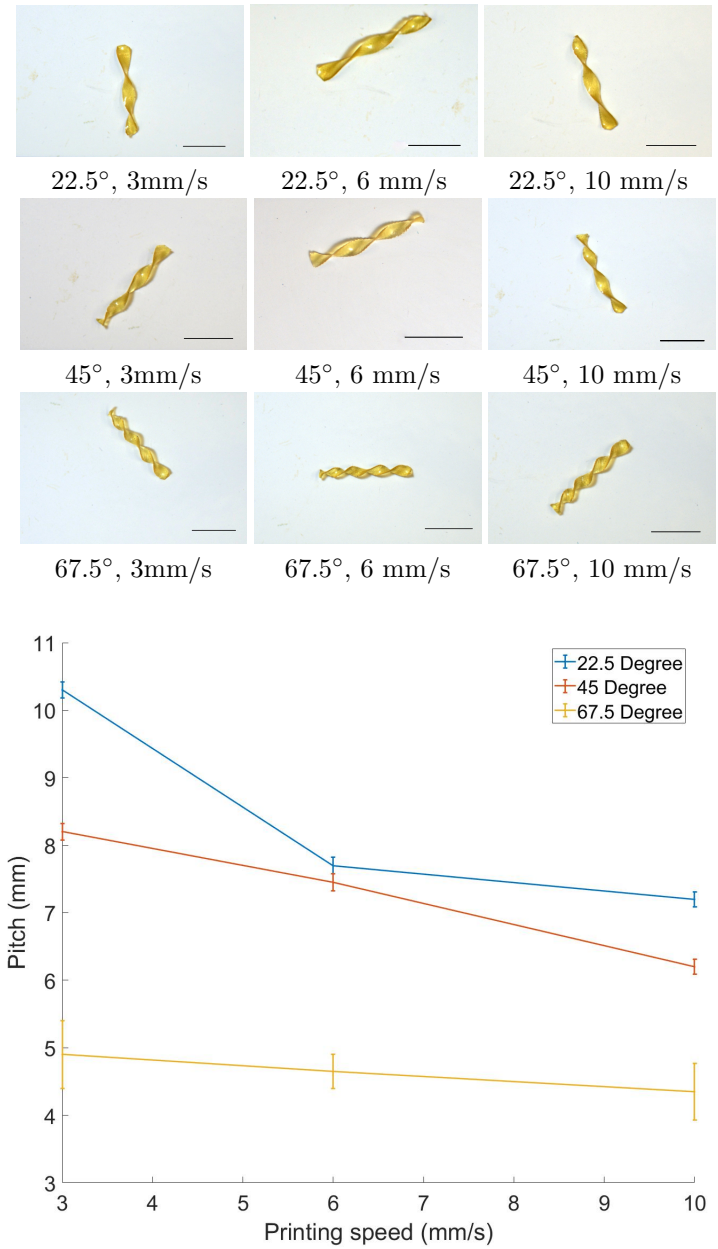

Figure 27: Pitches for helices printed at different speeds and angles. The error bars signify one standard deviation. Scale bar = 10mm

4.2 4D Printed LCE Hinges

A hinge is a mechanical bearing that connects two machine parts and allows a limited angle of rotation between them. Hinges have previously been manufactured using 4D printing technology [108, 109] but multiple materials were used to prepare those hinges. In this study, we manufactured fully functional hinges printing LCE only. In Chapter II we have shown how printing speed and printing angle affect the actuation of 4D printed LCEs. We have combined these effects to fabricate hinges that are capable of bending at controlled

angles and suited for different purposes.

4.2.1 Hinge Preparation and Testing Method

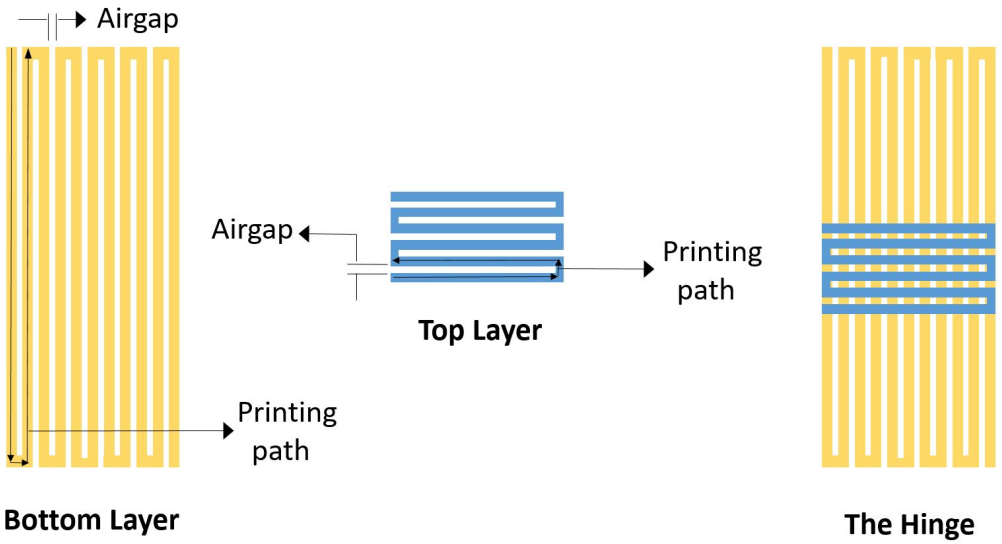

a)Printing mechanism of the bi-layer hinge

b)The 4D printed LCE hinge at undeformed, neutral state

Figure 28: Printing mechanism of the LCE hinge and the finished product

The hinges have two orthogonally printed layers, a bigger bottom layer and a smaller top layer (Figure 28) as demonstrated by Ren et. al. [17]. The top layer contraction that bends the bottom layer. The bottom layer is printed at 0° printing angle and 0.5 mm/s printing speed. The UV LEDs that create instantaneous curing is turned off while printing the bottom layer. The goal for the bottom layer is to keep actuation at a minimum hence the low printing speed and no instantaneous curing. The UV LEDs is turned on while printing the top layer as that layer is required to generate enough actuation strain. The top layer is printed at 90° printing angle, orthogonal to the printing direction of the bottom layer. The rectangular hinge specimens are 33 mm long and 15 mm wide.There are two factors that can affect the degree of the bending induced by the hinges— the printing speed of the top layer

and the width of the hinge. In order to investigate how these factors affect the bending of the hinges, we prepared the following hinge specimens:

- 1.5 mm wide hinges printed at 3, 6, 8, 10 and 12 mm/s speeds.
- 3 mm wide hinges printed at 3, 6, 8, 10 and 12 mm/s speeds.
- 1.5, 2, 2.5, 3, 3.5 and 4 mm wide hinges printed at 8 mm/s speed.

For both the top and bottom layers, the airgap was 0 mm and printing temperature was 50°C.

The hinge specimens were tested on a heater plate at 95°C. A flat load was placed on one end of the hinge and the other end could bend freely. Photos of the bent hinges were taken and the angles of bending were measured via Matlab image processing. We measured the bending angle of the hinges as the angle between the grounded end and the elevated end of the hinge. So if a hinge has a low bending angle that means the hinge is capable of generating a high amount of bending deformation. When the bending angle is 0, the two ends of the hinge are in contact with each other. We measured the angle for each hinge 5 times and the mean and the standard deviation of the measurements were plotted via Matlab.

4.2.2 Results and Discussion

Upon heating, the loaded end stays grounded while the other end is elevated from the heater plate floor. We measured the bending angle of the hinges as the angle between the grounded end and the elevated end of the hinge. So if a hinge has a low bending angle that means the hinge is capable of generating a high amount of bending deformation. When the bending angle is 0°, the two ends of the hinge are in contact with each other. Figure 29 shows that if the hinge width is unchanged, the bending angle of the hinges decrease with the increase in printing speed that means the hinges bend more as the printing speed increases. Figure 30 shows that at constant printing speed, the bending angle of the hinges increase with the increase in hinge width. A 4 mm-wide hinge printed at 8 mm/s bends with a bending angle of 0°.

The hinge specimens consist of two orthogonally printed layers. As the bottom layer is printed at 0.5 mm/s, the actuation is extremely low. The top layer is printed at higher speeds. The difference in actuation strain between the two layers creates the bending. In chapter II, we demonstrated that the specimens printed at 90° printing angle coils up. Similarly, the upper layer printed at 90° induces the bending motion, effectively creating a hinge. This principle has been used to manufacture the hinge specimens. With the increase in printing speed, the bending actuation of the upper layer increases hence the hinges have a higher bending angle at higher printing speeds. The angle of bending is highly dependent on the width of the hinges as the bending force generated increases with the width (Figure 30).

The LCE hinges used in this study are different from other 4D printed hinges because they are comprised of only one material. In previous studies, multi-material 4D hinges were manufactured and at least one active material along with a rigid material was used in order to manufacture those hinges [108, 109]. The active materials used in those hinges were capable of bending with the application of a stimulus but as the rigid materials were connected with the stimulus-responsive active materials, bending was induced in the rigid materials too.

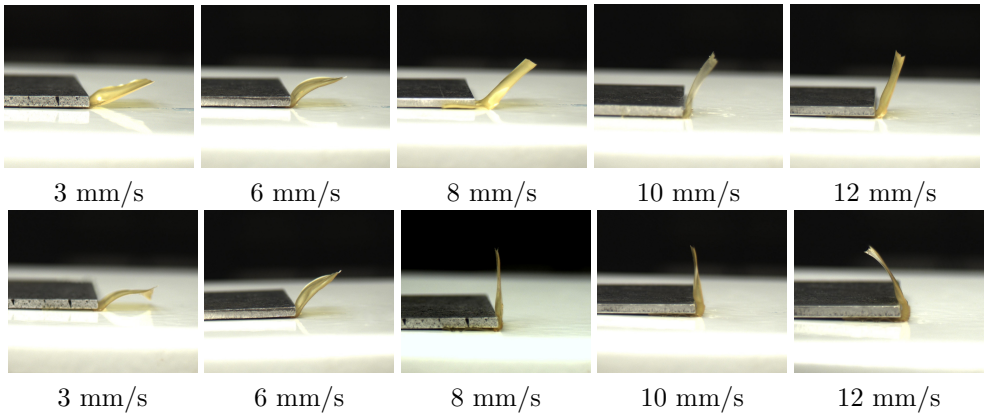

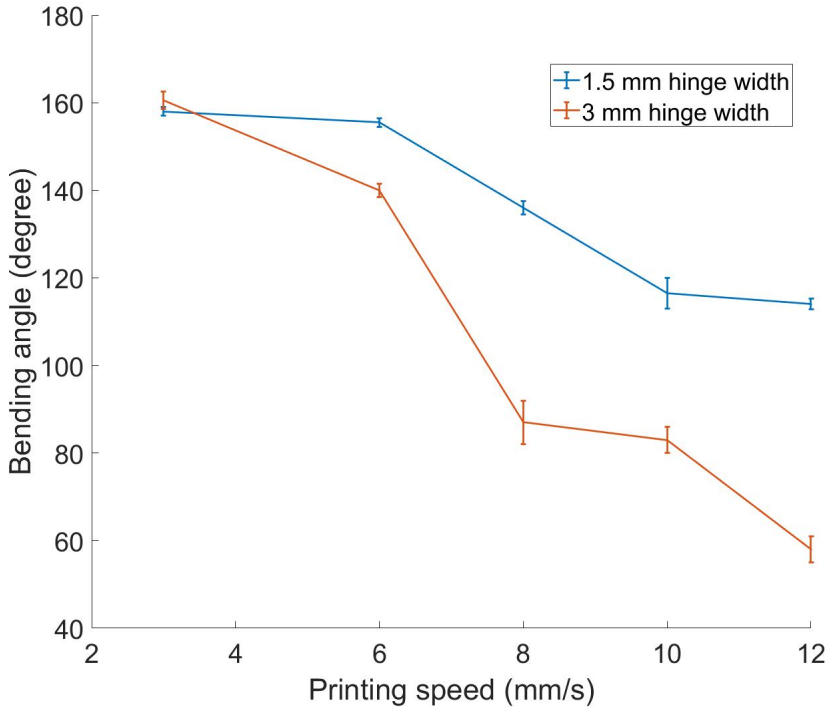

Figure 29: Bending angles for 1.5 and 3 mm wide hinges printed at different speeds. Hinge width for the 1st row of hinges is 1.5 mm and 3 mm for the second row. Error bars signify 1 standard deviation

In case of 4D printed LCE hinges, the need for multiple materials have been eliminated as LCEs can be used as both active and rigid material by varying the printing parameters. The bottom layer of the LCE hinge is printed at a very slow speed to keep the actuation in that layer at a minimum. So the bottom layer basically acts as the rigid material as it shows little response to the application of heat. On the other hand, the top layer is printed at higher speeds and is more susceptible to stimulus-responsive bending. This is how 4D-printed LCE hinges negate the necessity of using multiple materials.

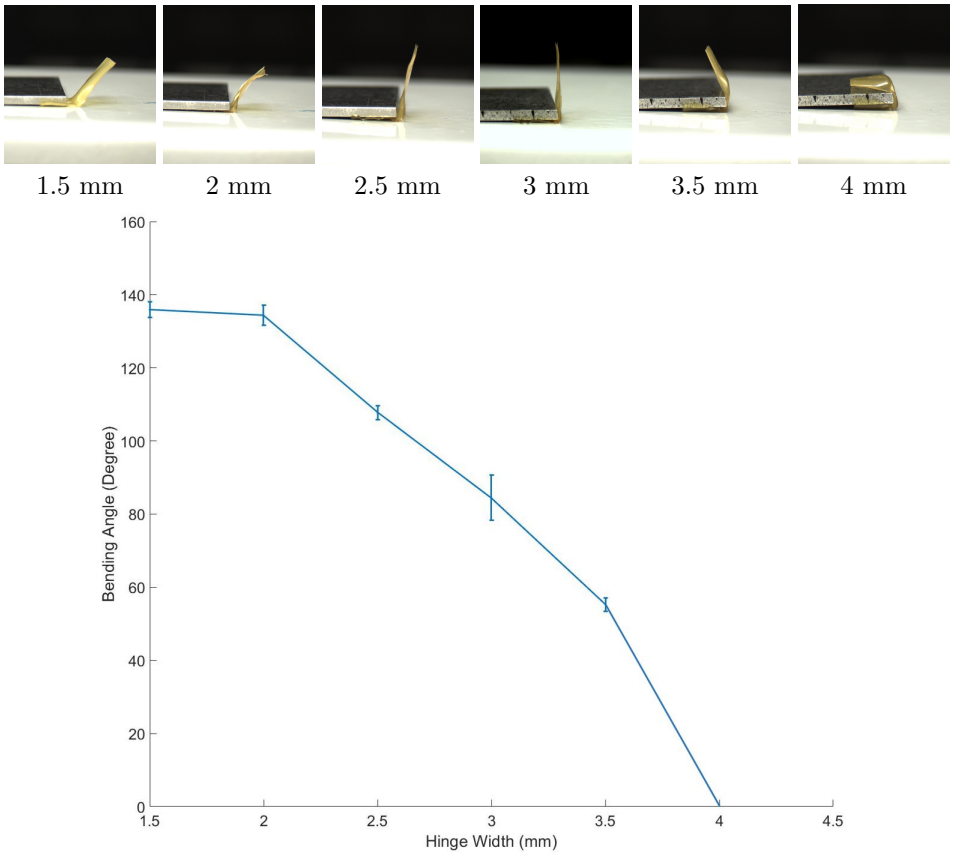

Figure 30: Bending angles for hinges printed at 8 mm/s speed. Error bars signify 1 standard deviation

4.3 Self-folding LCE Box

We manufactured a 4D printed LCE box capable of folding and unfolding in and out of a box shape with the application of heat. The box is basically a soft robot as conventional digital or electrical means have not been used to trigger the actuation of the box. Heat and material programming have been used to reciprocate between two programmed shapes. The self-folding box is an example of 2D-to-3D deformation. 4D printed self-folding boxes have been manufactured in various studies before but multiple materials were used in those studies [110, 79, 109]. In this study, we proposed a design where only one material can be used to prepare both the active and rigid parts of the self-folding box. We used printing conditions and directions to locally program the self-folding box and trigger site-specific actuation.

4.3.1 Specimen Preparation and Testing Method

The box uses the hinges discussed in section 4.2. Four hinges have been used in order to trigger the folding mechanism. At its unfolded, unheated state, the box is a 2D shape as shown in figure 31. The box consists of two layers where the bottom layer is passive and the top layer is active and acts as hinges. The bottom layer is printed at 0.5 mm/s as shown in figure 31 and the top layer is printed at 8 mm/s. The top layer's printing direction is

orthogonal with respect to the bottom layer direction which means if part of the bottom layer is printed at 0° printing angle, the layer that goes on top of that part is printed at 90° printing angle and vice versa. The printing temperature was 50°C, the airgap was 0 mm, layer height was 0.1 mm. The dimensions are shown in 31. The width of the hinges are 3 mm. This specific printing speed and the hinge width were chosen in order to trigger the desired amount of bending (right angle bending) in every side of the self-folding box. As we require the bottom layer to act passive and have as low actuation as possible, the UV LEDs creating instantaneous curing were turned off while printing the bottom layer. The UV LEDs were turned on while printing the top layer as that layer is required to generate enough actuation strain.

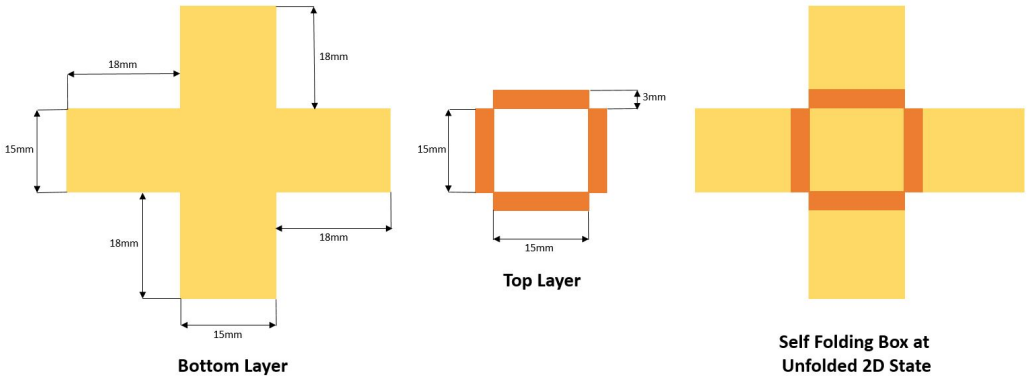

Figure 31: Dimensions and printing pattern of the 4D-printed self-folding box

To trigger the self-folding mechanism, the box was placed on a heater plate surface at 95°C temperature. A cylindrical weight of 15 grams was placed at the center of the box to provide stability while actuating. The weight also eliminates unwarranted bending and crinkles in the structure and ensures proper actuation of the hinges. The folding of the box was video taped and photos were taken from various angles.

4.3.2 Results And Discussion

When the box along with a small weight at its center are heated on the heater plate, all of the 4 hinges generate a bending motion that folds the sides of the box as shown in 32. The hinge mechanism works because of the site-specific material programming. The orthogonally printed bi-layer hinges induce a bending motion in the structure upon heating and the working principles of 4D printed LCE hinges have been demonstrated in section 4.2. The bottom layer of the structure was printed at a very low printing speed of 0.5 mm/s without UV LED lights and thus the actuation of the bottom layer was programmed to be kept as low as possible. So the bottom layer serves as the faces of the box. The hinges or the stimulus-responsive active parts of the structure are required to have a much higher actuation strain compared to the passive parts.

For the structure to work like a proper self-folding box, the hinges need to bend the rigid sides of the box at a right angle. So if the actuation strain generated by the hinges

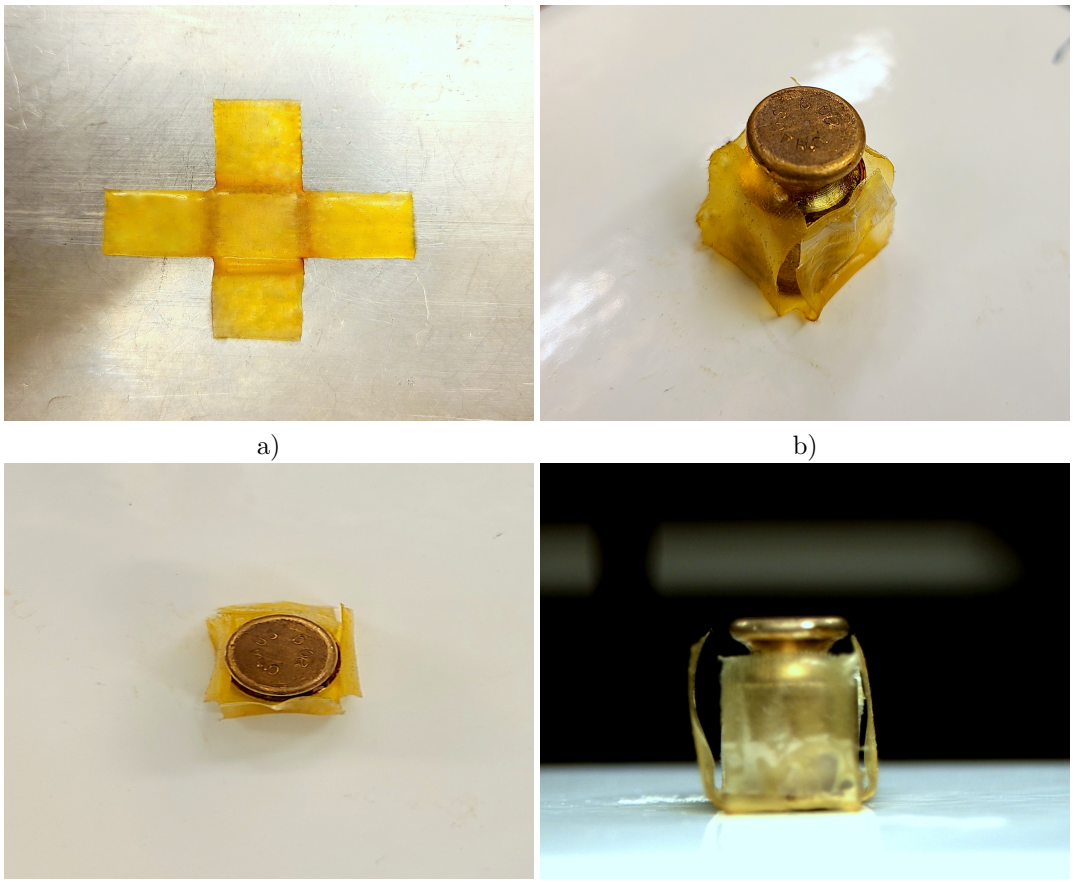

Figure 32: a) the self folding box at unheated, unfolded 2D state. b) Isometric view of the self folding box after actuation. c) Top view of the self folding box. d) Side view of the self-folding box

happens to be too low, the sides of the box will not bend enough to form a right angle with the base and if the actuation strain is too high, bending will be more than 90° and the deformation of the hinges will lean more towards folding than bending. So to induce just the right amount of bending in the hinges, specific printing parameters were used. As we learned from our study on hinges in section 4.2, 3 mm-wide hinges printed at 8 mm/s are optimum for generating a 90° bend. These specific printing parameters were used to print all the hinges. The transformation of the box is reversible so the construction and deconstruction of the box depends only upon the temperature.

Multimaterial 4D printed self-folding boxes have been manufactured in the previous studies [110, 109]. Liu et al. [110] manufactured a sequentially self-folding box made of polymer sheets and light absorbing, heat activated hinges. A desktop 3D printer was used to print black ink onto the shape-memory polymer sheets, followed by irradiation with light. The inked regions on the specimen preferentially absorbed the light and converted it into heat, which, in turn, caused a localized gradient of shrinkage across the thickness of the polymer sheet and generated bending within seconds [109]. Mao et. al. also manufactured a multimaterial, sequential self-folding box realized by thermal activation of spatially-variable

patterns that was 3D printed with digital shape memory polymers. The time-dependent behavior of each polymer facilitated the temporal sequencing of activation when the structure was subjected to a uniform temperature. Roach et. al. used 4D printed LCEs to manufacture self-folding boxes where LCE was used as the active material along with a stimulus non-responsive rigid material. In our study, we bypassed the use of multiple materials as we used the same material for printing the active and passive parts under different printing conditions. We obtained a box with controlled 90 degrees hinges.

CHAPTER V

Application to Soft Robotics: Actuation Programmed Through the Printing Path

5.1 4D Printed LCE Grid

We have seen in chapter II how actuation works for LCE strips printed along X direction. Unlike rectangular strips, a grid is printed both along X and Y directions so the printed filaments are oriented perpendicularly to each other. A grid has mutliple empty pockets of space in between parallel lines and it also has overlapping filaments. The grid exhibits 2D-to-2D deformation. The goal of studying the 4D printed LCE grid is to find out how the grid actuates along both the X and Y axes and how the overlapping parts and empty pockets affect the actuation.

5.1.1 Specimen Preparation and Testing Method

The LCE grid is a square structure of 21 mm by 21 mm dimensions. The intersecting lines in the grid are 1 mm thick and 3 mm apart from one another (33). The grid has only one layer but there is overlapping at the intersection of the lines. The grid was printed at 50°C temperature, 0 mm airgap, 10 mm/s printing speed, .1 mm layer height.

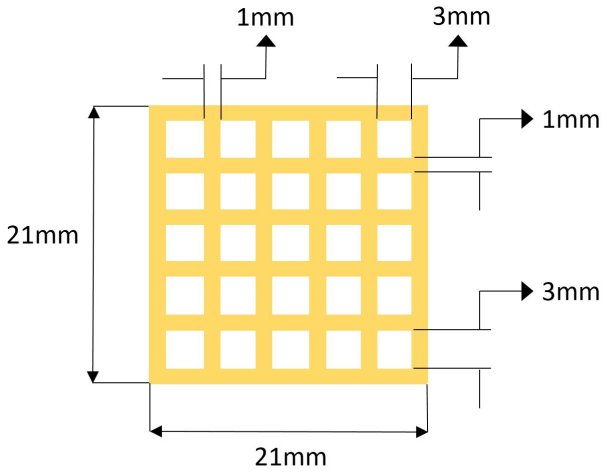

Figure 33: Dimensions of the 4D printed LCE grid

To measure the actuation, the grid specimen was placed on a heater plate coated with silicon oil. The temperature of the plate was kept at 95°C. The change in shape of the grid

was recorded with a video camera and the actuation strain was quantified by processing the images in MATLAB.

5.1.2 Results and Discussion

The grid exhibits both longitudinal and lateral contraction when heated at 95°C. The longitudinal and lateral strains were measured to be 37.50% and 25.38% respectively. The overlapping parts of the grid acted like miniature hinges as they had orthogonally printed fibers. In the study on hinges in section 4.2, we found that orthogonally printed layers tend to generate a bending motion. Even though there is some localised bending due to the overlapping fibers acting like hinges, the overall structure does not bend globally. The whole grid basically shrinks into a smaller grid due to the actuation.

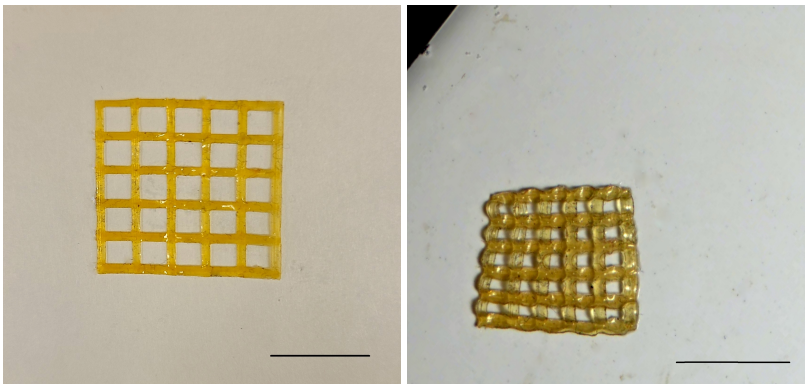

a) b)

Figure 34: 4D printed LCE grid (a) before actuation and (b) after actuation. Scale bar = 10 mm

4D printed LCE grids were previously studied in multiple occasions in different capacities [14, 76, 78, 17, 80]. While Kotikian et. al.[78] prepared a 4D printed LCE mesh-shaped grid that shrank into an isotropic form, Ren et. al.[17] printed an LCE grid that could bend globally and form a porous cylinder. Ren et. al. used bi-layered orthogonal printing paths with varied printing speeds to achieve a 360° bending of the LCE grid. In case of the grid we manufactured in this study, the actuation pattern is consistent with the actuation of the rectangular LCE strips discussed in chapter II and the hinges discussed in section 4.2.

5.2 4D Printed LCE Pyramid

In our attempt to manufacture structures capable of complex, reversible shape-morphing, we printed a flat, LCE square that can assume the shape of a pyramid when heated. This is another example of a 2D-to-3D deformation. This complex shape-shifting structure was programmed by controlling the printing paths in an orderly manner.

5.2.1 Specimen Preparation and Testing Method

The specimen was printed in a square spiral pattern as shown in figure 35. The single layer square spiral shape had 0 mm airgap and its dimensions were 15 mm by 15 mm. To achieve

a high actuation strain, a high printing speed of 10 mm/s was used. The layer height was

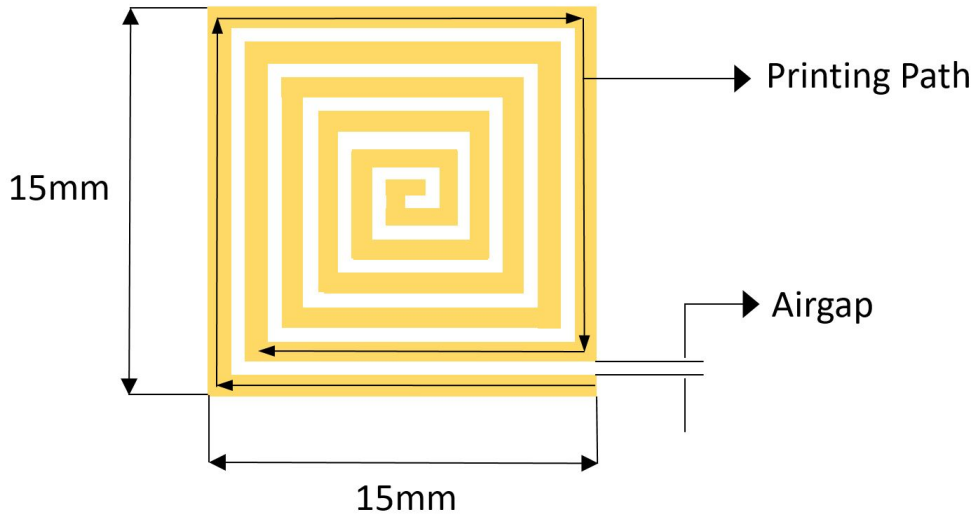

Figure 35: Dimensions and printing pattern of the LCE pyramid

0.1 mm and printing temperature was 50°C. The specimen was heated on a heater plate and photos were taken as the flat square shape-morphed into a pyramid. The images were then processed in Matlab to measure the height of the pyramid.

5.2.2 Results and Discussion

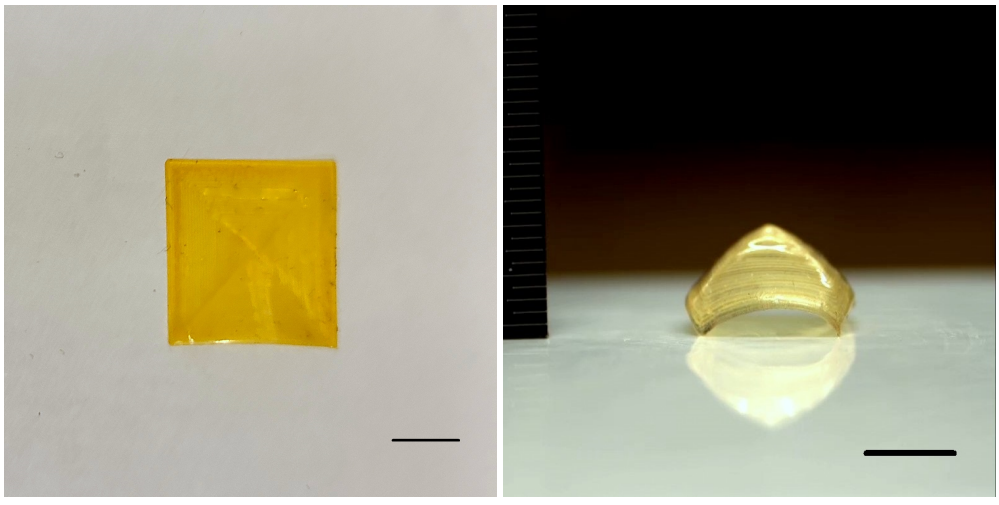

a) b)

Figure 36: 4D printed LCE pyramid before actuation (a) and after actuation (b). The black scale bar: 5mm

When heat is applied, the 2D LCE square undergoes an out-of-plane deformation. After actuation, the distance from the heater plate is higher at the center of the LCE square than the peripheral regions and thus the pyramid structure is formed. The printing path and the high printing speed are the reasons for this particular type of shape change. The actuation strain is high in the printed fibers because of the high printing speed. Actuation takes place along the direction of the printed fibers which causes the LCE square to move upward and the upward movement is the highest at the center of the triangle. As a result of this unique actuation pattern, the sides or the fringe of the square LCE strip form the base of the pyramid and the center of the square forms the capstone of the pyramid. The height of the pyramid is measured to be 7.64 mm which means the center of the square is elevated 7.64 mm from the heater plate surface.

Pyramid shapes were not 4D-printed in previous studies but 4D printed LCE cones were manufactured in several studies before [78, 80]. Kotikian et al. [78] printed a series of concentric squares which collectively would assume the shape of a cone after actuation. Saed et al. [80] printed a circular spiral using two different materials that could transform into a conical shape upon actuation . In both studies, higher printing speed was used to attain maximum possible actuation. In our study, we used the same printing principles to attain the pyramid shape with a square base and a unique printing path.

CHAPTER VI

Conclusion and Future Works

6.1 Conclusion

Inducing shape-morphing properties in additively manufactured objects requires more precision and parameter optimization than mere additive manufacturing. One of our primary objectives of this study was to find out the optimal parameters and printing conditions for the 4D printing of LCEs. The LCP ink becomes too viscous to be pushed out of the nozzle at lower printing temperatures. The ink loses viscosity at higher temperatures which keeps the filament from holding itself once printed. We found that 50°C is the optimum temperature for the 4D printing of LCE. We also found that 0.1 mm is the optimum nozzle-to-bed distance that provides enough tensile force for the proper alignment of mesogens.

One of the objectives of our study was to find out how different properties of 4D-printed LCEs are influenced by printing parameters and how those properties differ from bulk LCEs. We found that 4D printed LCEs exhibit actuation properties and the actuation is significantly affected by printing speed and angle. Actuation strain increases with the increase in printing speed and bending increases with the rise in printing angle. From polarised light microscope images, we observed that the mesogens are more aligned at higher printing speeds and the enhanced alignment of mesogens results in higher actuation strain. We found that the actuation strain does not change significantly above 10 mm/s printing speed but we have not printed at speeds over 12 mm/s to conclude whether the actuation strain remains unchanged at very high printing speeds. We have demonstrated how the actuation strain and bending can be controlled in 4D-printed LCEs by regulating readily accessible printing parameters like printing speed and angle.

We explored how mechanical properties of 4D printed are influenced by printing parameters. The Young's modulus of 4D printed LCEs first increases then decreases with the increase in printing speed. The loss and storage modulus also rise and then drop with the increase in printing speed. Better alignment of mesogens is attained at higher printing speeds and more aligned mesogens induce more stiffness in the material explaining why the storage modulus and Young's modulus initially increase with the increase in printing speed. But if the printing speed is above 8 mm/s, the printed filaments lose continuity and uniformity which lead to reduced storage modulus and young's modulus. Moreover, 4D printed LCEs exhibit a significantly higher Young's modulus, loss modulus and storage modulus compared to bulk LCEs. We conducted all the experiments on unstretched bulk LCE specimens so we can't conclude whether stretched bulk LCEs, where the mesogen alignment are enhanced, exhibit mechanical properties that closely resemble 4D-printed LCEs. LCEs printed at different angles exhibit a lower Young's modulus, storage and loss modulus with the increase

in printing angle.

One of the goals of this study was to explore the potential application of 4D printed LCEs in soft robotics via complex actuating structures. We explored different modes of material programming like layer orientation, varying printing paths to attain complex actuation. We fabricated two orthogonally printed layers of LCEs to create a hinge which has a lot of applications in the field of soft robotics. We found that we could precisely control the bending angle of the hinges by controlling the hinge width and printing speed. By using 4 hinges with controlled bending angles, we manufactured a self-folding box capable of folding and unfolding into a box shape without any conventional means of robotics like electrical or digital signals. By varying the printing conditions, we created active and passive zones within the printed structure without using multiple materials and using only heat as stimulus for triggering actuation. We also printed LCE helices to demonstrate 2D-to-3D deformation by printing two layers at supplementary angles. We controlled the pitch of the helices with two parameters— printing angle and printing speed. We also printed a 2D square spiral that can assume the shape of a pyramid when heated. When the square spiral shape is heated, a pyramid shape is formed as the center of the square becomes the pyramidion and the sides of the square act as the base. We manufactured complex actuating shapes with predictable and precise control but we could not attain the level of control and precision of conventional robotics. We have used printing speed, printing path and layer orientations as the drivers of controlled and reversible in-plane and out-of-plane deformation in multiple directions.

6.2 Future Work

Many aspects of 4D printing of LCEs need further investigation, such as exploring different ink formulations, the effect of printing parameters, the feasibility of more complex prints, and the mechanical and actuation properties of the printed material.

We have used only one type of LCE ink to manufacture all the specimens in this study. In the future, we can work with different types of LCEs with different actuating properties. For example, we can work with LCEs that can actuate by getting heated from absorbed light. This will allow us to control the actuation more precisely and we can use concentrated light beams to trigger actuation in certain parts of the structure while the rest of the structure is deliberately kept from actuating.

We have investigated how various printing conditions, like printing speed or printing angle, affect the actuation of 4D printed LCEs. However, all specimens were printed at a constant temperature of 50°C. The influence of printing temperature on the actuation strain and properties of the printed specimen should be explored as well.

We have only observed the actuation of single layer or bi-layer 4D printed LCEs. We have not printed any structure with negative airgaps or overlapping printed fibers. More complex LCE structures consisting of more than 2 layers and a negative airgap should be explored.

We have measured the actuation strain via image processing. But we do not know how much actuation force has been generated in the specimens. In order for 4D printed LCEs to be used in more sophisticated fields of soft robotics, we need to know precisely the amount of force being generated during the actuation. Future studies should address this issue and conduct a study to measure the actuation force or power developed.

We have conducted DMA and tensile tests to characterize the mechanical and viscoelastic properties of 4D printed LCEs. But we did not perform measurements in compression or in different directions to assess anisotropy. So some mechanical and viscoelastic properties of 4D printed LCEs are still unexplored. Besides, we performed the mechanical characterization at room temperature. We are yet to determine the influence of temperature on the mechanical and viscoelastic properties of 4D printed LCEs. In future, studies can be carried out in order to find out the influence of temperature on various mechanical properties of 4D printed LCEs.

We have explored some soft robotic applications of 4D printed LCEs. But 4D printed LCEs have the potential to be used more prolifically in the field of soft robotics. We designed a self-folding box where the hinges of the box are activated all at once. We can introduce sequential folding to the box by heating the hinges in a certain order. To achieve that, we can use conductive wires that can generate Joule heating in the hinges in any desired order. The hinges we manufactured can be modified to be used as soft robotic grippers to lift lightweight objects. We did not explore the potential of 4D printed LCEs being used in multimaterial printing. In future studies, 4D printed LCEs can be used in combination with other materials to create more complex designs.

REFERENCES

[1] A. Sydney Gladman, E. A. Matsumoto, R. G. Nuzzo, L. Mahadevan, and J. A. Lewis, "Biomimetic 4D printing," *Nature Materials*, vol. 15, pp. 413–418, Apr. 2016.

[2] Q. Ge, A. H. Sakhaei, H. Lee, C. K. Dunn, N. X. Fang, and M. L. Dunn, "Multimaterial 4D Printing with Tailorable Shape Memory Polymers," *Scientific Reports*, vol. 6, p. 31110, Aug. 2016.

[3] S. Tibbits, "4D Printing: Multi-Material Shape Change," *Architectural Design*, vol. 84, pp. 116–121, Jan. 2014.

[4] G. Villar, A. D. Graham, and H. Bayley, "A Tissue-Like Printed Material," *Science*, vol. 340, pp. 48–52, Apr. 2013.

[5] F. Brömmel, D. Kramer, and H. Finkelmann, "Preparation of Liquid Crystalline Elastomers," in *Liquid Crystal Elastomers: Materials and Applications* (W. H. de Jeu, ed.), Advances in Polymer Science, pp. 1–48, Berlin, Heidelberg: Springer, 2012.

[6] C. Yakacki, "Journal club: Overcoming challenges in mechanically actuating liquid-crystalline elastomers — imechanica." `https://imechanica.org/node/16853`.

[7] T. A. Campbell, S. Tibbits, and B. Garrett, "The Programmable World," *Scientific American*, vol. 311, no. 5, pp. 60–65, 2014.

[8] Z. Ding, C. Yuan, X. Peng, T. Wang, H. J. Qi, and M. L. Dunn, "Direct 4D printing via active composite materials," *Science Advances*, vol. 3, p. e1602890, Apr. 2017.

[9] S. T. Ly and J. Y. Kim, "4D printing – fused deposition modeling printing with thermal-responsive shape memory polymers," *International Journal of Precision Engineering and Manufacturing-Green Technology*, vol. 4, pp. 267–272, July 2017.

[10] H. Yang, W. R. Leow, T. Wang, J. Wang, J. Yu, K. He, D. Qi, C. Wan, and X. Chen, "3D Printed Photoresponsive Devices Based on Shape Memory Composites," *Advanced Materials*, vol. 29, no. 33, p. 1701627, 2017.

[11] A. Nishiguchi, H. Zhang, S. Schweizerhof, M. F. Schulte, A. Mourran, and M. Möller, "4D Printing of a Light-Driven Soft Actuator with Programmed Printing Density," *ACS Applied Materials & Interfaces*, vol. 12, pp. 12176–12185, Mar. 2020.

[12] D. Raviv, W. Zhao, C. McKnelly, A. Papadopoulou, A. Kadambi, B. Shi, S. Hirsch, D. Dikovsky, M. Zyracki, C. Olguin, R. Raskar, and S. Tibbits, "Active Printed Materials for Complex Self-Evolving Deformations," *Scientific Reports*, vol. 4, p. 7422, Dec. 2014.

[13] F. Momeni, S. M.Mehdi Hassani.N, X. Liu, and J. Ni, "A review of 4D printing," *Materials & Design*, vol. 122, pp. 42–79, May 2017.

[14] C. Zhang, X. Lu, G. Fei, Z. Wang, H. Xia, and Y. Zhao, "4D Printing of a Liquid Crystal Elastomer with a Controllable Orientation Gradient," *ACS Applied Materials & Interfaces*, vol. 11, pp. 44774–44782, Nov. 2019.

[15] Y. Y. C. Choong, S. Maleksaeedi, H. Eng, J. Wei, and P.-C. Su, "4D printing of high performance shape memory polymer using stereolithography," *Materials & Design*, vol. 126, pp. 219–225, July 2017.

[16] M. Taheri Andani, S. Saedi, A. S. Turabi, M. R. Karamooz, C. Haberland, H. E. Karaca, and M. Elahinia, "Mechanical and shape memory properties of porous Ni50.1Ti49.9 alloys manufactured by selective laser melting," *Journal of the Mechanical Behavior of Biomedical Materials*, vol. 68, pp. 224–231, Apr. 2017.

[17] L. Ren, B. Li, Y. He, Z. Song, X. Zhou, Q. Liu, and L. Ren, "Programming Shape-Morphing Behavior of Liquid Crystal Elastomers via Parameter-Encoded 4D Printing," *ACS Applied Materials & Interfaces*, vol. 12, pp. 15562–15572, Apr. 2020.

[18] T. van Manen, S. Janbaz, and A. A. Zadpoor, "Programming 2D/3D shape-shifting with hobbyist 3D printers," *Materials Horizons*, vol. 4, no. 6, pp. 1064–1069, 2017.

[19] J. A. Lewis, "Direct Ink Writing of 3D Functional Materials," *Advanced Functional Materials*, vol. 16, no. 17, pp. 2193–2204, 2006.

[20] M. A. Skylar-Scott, S. Gunasekaran, and J. A. Lewis, "Laser-assisted direct ink writing of planar and 3d metal architectures," *Proceedings of the National Academy of Sciences*, vol. 113, no. 22, pp. 6137–6142, 2016.

[21] L. L. Lebel, B. Aissa, M. A. E. Khakani, and D. Therriault, "Ultraviolet-assisted direct-write fabrication of carbon nanotube/polymer nanocomposite microcoils," *Advanced Materials*, vol. 22, no. 5, pp. 592–596, 2010.

[22] J. T. Muth, P. G. Dixon, L. Woish, L. J. Gibson, and J. A. Lewis, "Architected cellular ceramics with tailored stiffness via direct foam writing," *Proceedings of the National Academy of Sciences*, vol. 114, no. 8, pp. 1832–1837, 2017.

[23] M. A. Skylar-Scott, J. Mueller, C. W. Visser, and J. A. Lewis, "Voxelated soft matter via multimaterial multinozzle 3d printing," *Nature*, vol. 575, no. 7782, pp. 330–335, 2019.

[24] J. E. Smay, J. Cesarano, and J. A. Lewis, "Colloidal inks for directed assembly of 3-d periodic structures," *Langmuir*, vol. 18, no. 14, pp. 5429–5437, 2002.

[25] J. E. Smay, G. M. Gratson, R. F. Shepherd, J. Cesarano III, and J. A. Lewis, "Directed colloidal assembly of 3d periodic structures," *Advanced Materials*, vol. 14, no. 18, pp. 1279–1283, 2002.

[26] T. Zhao, R. Yu, X. Li, B. Cheng, Y. Zhang, X. Yang, X. Zhao, Y. Zhao, and W. Huang, "4D printing of shape memory polyurethane via stereolithography," *European Polymer Journal*, vol. 101, pp. 120–126, Apr. 2018.

[27] S. C. Ligon, R. Liska, J. Stampfl, M. Gurr, and R. Mülhaupt, "Polymers for 3D Printing and Customized Additive Manufacturing," *Chemical Reviews*, vol. 117, pp. 10212–10290, Aug. 2017.

[28] Z. Zhao, J. Wu, X. Mu, H. Chen, H. J. Qi, and D. Fang, "Origami by frontal photopolymerization," *Science Advances*, vol. 3, p. e1602326, Apr. 2017.

[29] L. Huang, R. Jiang, J. Wu, J. Song, H. Bai, B. Li, Q. Zhao, and T. Xie, "Ultrafast Digital Printing toward 4D Shape Changing Materials," *Advanced Materials*, vol. 29, no. 7, p. 1605390, 2017.

[30] Z. Zhang, K. G. Demir, and G. X. Gu, "Developments in 4D-printing: A review on current smart materials, technologies, and applications," *International Journal of Smart and Nano Materials*, vol. 10, pp. 205–224, July 2019.

[31] Y. Zhou, W. M. Huang, S. F. Kang, X. L. Wu, H. B. Lu, J. Fu, and H. Cui, "From 3D to 4D printing: Approaches and typical applications," *Journal of Mechanical Science and Technology*, vol. 29, pp. 4281–4288, Oct. 2015.

[32] J. Zhou and S. S. Sheiko, "Reversible shape-shifting in polymeric materials," *Journal of Polymer Science Part B: Polymer Physics*, vol. 54, no. 14, pp. 1365–1380, 2016.

[33] C. Liu, H. Qin, and P. T. Mather, "Review of progress in shape-memory polymers," *Journal of Materials Chemistry*, vol. 17, no. 16, pp. 1543–1558, 2007.

[34] D. Ratna and J. Karger-Kocsis, "Recent advances in shape memory polymers and composites: A review," *Journal of Materials Science*, vol. 43, pp. 254–269, Jan. 2008.

[35] Q. Zhang, D. Yan, K. Zhang, and G. Hu, "Pattern Transformation of Heat-Shrinkable Polymer by Three-Dimensional (3D) Printing Technique," *Scientific Reports*, vol. 5, p. 8936, Mar. 2015.

[36] F. Liu, C. Vyas, G. Poologasundarampillai, I. Pape, S. Hinduja, W. Mirihanage, and P. J. Bartolo, "Process-Driven Microstructure Control in Melt-Extrusion-Based 3D Printing for Tailorable Mechanical Properties in a Polycaprolactone Filament," *Macromolecular Materials and Engineering*, vol. 303, no. 8, p. 1800173, 2018.

[37] H. Wei, Q. Zhang, Y. Yao, L. Liu, Y. Liu, and J. Leng, "Direct-write fabrication of 4d active shape-changing structures based on a shape memory polymer and its nanocomposite," *ACS applied materials & interfaces*, vol. 9, no. 1, pp. 876–883, 2017.

[38] X. Kuang, D. J. Roach, J. Wu, C. M. Hamel, Z. Ding, T. Wang, M. L. Dunn, and H. J. Qi, "Advances in 4D Printing: Materials and Applications," *Advanced Functional Materials*, vol. 29, no. 2, p. 1805290, 2019.

[39] Q. Zhang, K. Zhang, and G. Hu, "Smart three-dimensional lightweight structure triggered from a thin composite sheet via 3D printing technique," *Scientific Reports*, vol. 6, p. 22431, Feb. 2016.

[40] J. P. Jung, D. B. Bhuiyan, and B. M. Ogle, "Solid organ fabrication: Comparison of decellularization to 3D bioprinting," *Biomaterials Research*, vol. 20, p. 27, Aug. 2016.

[41] A. Khademhosseini and R. Langer, "A decade of progress in tissue engineering," *Nature Protocols*, vol. 11, pp. 1775–1781, Oct. 2016.

[42] M. Zarek, N. Mansour, S. Shapira, and D. Cohn, "4D Printing of Shape Memory-Based Personalized Endoluminal Medical Devices," *Macromolecular Rapid Communications*, vol. 38, no. 2, p. 1600628, 2017.

[43] D. L. Taylor and M. in het Panhuis, "Self-Healing Hydrogels," *Advanced Materials*, vol. 28, no. 41, pp. 9060–9093, 2016.

[44] M. Warner and X. J. Wang, "Elasticity and phase behavior of nematic elastomers," *Macromolecules*, vol. 24, pp. 4932–4941, Aug. 1991.

[45] T. H. Ware, M. E. McConney, J. J. Wie, V. P. Tondiglia, and T. J. White, "Voxelated liquid crystal elastomers," *Science*, vol. 347, pp. 982–984, Feb. 2015.

[46] M. Yamada, M. Kondo, J.-i. Mamiya, Y. Yu, M. Kinoshita, C. J. Barrett, and T. Ikeda, "Photomobile Polymer Materials: Towards Light-Driven Plastic Motors," *Angewandte Chemie*, vol. 120, no. 27, pp. 5064–5066, 2008.

[47] J. M. Boothby, H. Kim, and T. H. Ware, "Shape changes in chemoresponsive liquid crystal elastomers," *Sensors and Actuators B: Chemical*, vol. 240, pp. 511–518, Mar. 2017.

[48] S. W. Ula, N. A. Traugutt, R. H. Volpe, R. R. Patel, K. Yu, and C. M. Yakacki, "Liquid crystal elastomers: An introduction and review of emerging technologies," *Liquid Crystals Reviews*, vol. 6, pp. 78–107, Jan. 2018.

[49] M. Warner and E. M. Terentjev, "Nematic elastomers—A new state of matter?," *Progress in Polymer Science*, vol. 21, pp. 853–891, Jan. 1996.

[50] C. Ohm, M. Brehmer, and R. Zentel, "Liquid Crystalline Elastomers as Actuators and Sensors," *Advanced Materials*, vol. 22, no. 31, pp. 3366–3387, 2010.

[51] P. G. de Gennes and J. Prost, *The Physics of Liquid Crystals*. Clarendon Press, 1993.

[52] P. J. Collings, M. R. Fisch, and M. A. Mooney, "Liquid Crystals: Nature's Delicate Phase of Matter," *American Journal of Physics*, vol. 60, pp. 958–958, Oct. 1992.

[53] H. Yu, *Dancing with Light: Advances in Photofunctional Liquid-Crystalline Materials*. CRC Press, Feb. 2015.

[54] F. Hardouin, N. Leroux, L. Noirez, P. Keller, M. Mauzac, and M. F. Achard, "Small Angle Neutron Scattering (Sans) Studies on "Side-On Fixed" Liquid Crystal Polymers," *Molecular Crystals and Liquid Crystals Science and Technology. Section A. Molecular Crystals and Liquid Crystals*, vol. 254, pp. 267–282, Sept. 1994.

[55] M. Warner and E. M. Terentjev, *Liquid Crystal Elastomers*. OUP Oxford, Apr. 2007.

[56] J. S. Biggins, M. Warner, and K. Bhattacharya, "Elasticity of polydomain liquid crystal elastomers," *Journal of the Mechanics and Physics of Solids*, vol. 60, pp. 573–590, Apr. 2012.

[57] K. Urayama, E. Kohmon, M. Kojima, and T. Takigawa, "Polydomain-Monodomain Transition of Randomly Disordered Nematic Elastomers with Different Cross-Linking Histories," *Macromolecules*, vol. 42, pp. 4084–4089, June 2009.

[58] J. R. Wolf, "Review: Main chain hydrogen-bonded liquid crystalline polymers," *Liquid Crystals Reviews*, vol. 2, pp. 28–46, Jan. 2014.

[59] J. D. Martin, C. L. Keary, T. A. Thornton, M. P. Novotnak, J. W. Knutson, and J. C. W. Folmer, "Metallotropic liquid crystals formed by surfactant templating of molten metal halides," *Nature Materials*, vol. 5, pp. 271–275, Apr. 2006.

[60] R. Zentel, "Liquid Crystalline Elastomers," *Angewandte Chemie*, vol. 101, no. 10, pp. 1437–1445, 1989.

[61] J. Küupfer and H. Finkelmann, "Liquid crystal elastomers: Influence of the orientational distribution of the crosslinks on the phase behaviour and reorientation processes," *Macromolecular Chemistry and Physics*, vol. 195, no. 4, pp. 1353–1367, 1994.

[62] S. M. Clarke, E. M. Terentjev, I. Kundler, and H. Finkelmann, "Texture Evolution during the Polydomain-Monodomain Transition in Nematic Elastomers," *Macromolecules*, vol. 31, pp. 4862–4872, July 1998.

[63] Y. Jia, B. Zhang, E. Zhou, Z. Feng, and B. Zang, "Synthesis and characterization of network liquid crystal elastomers and thermosets," *Journal of Applied Polymer Science*, vol. 85, no. 5, pp. 1104–1109, 2002.

[64] D. R. Merkel, R. K. Shaha, C. M. Yakacki, and C. P. Frick, "Mechanical energy dissipation in polydomain nematic liquid crystal elastomers in response to oscillating loading," *Polymer*, vol. 166, pp. 148–154, Mar. 2019.

[65] A. Sánchez-Ferrer and H. Finkelmann, "Thermal and mechanical properties of new Main-Chain Liquid-Crystalline Elastomers," *Solid State Sciences*, vol. 12, pp. 1849–1852, Nov. 2010.

[66] M. Warner, P. Bladon, and E. M. Terentjev, ""Soft elasticity" — deformation without resistance in liquid crystal elastomers," *Journal de Physique II*, vol. 4, pp. 93–102, Jan. 1994.

[67] A. Azoug, V. Vasconcellos, J. Dooling, M. Saed, C. M. Yakacki, and T. D. Nguyen, "Viscoelasticity of the polydomain-monodomain transition in main-chain liquid crystal elastomers," *Polymer*, vol. 98, pp. 165–171, Aug. 2016.

[68] S. Dey, D. M. Agra-Kooijman, W. Ren, P. J. McMullan, A. C. Griffin, and S. Kumar, "Soft Elasticity in Main Chain Liquid Crystal Elastomers," *Crystals*, vol. 3, pp. 363–390, June 2013.

[69] G. Skačej and C. Zannoni, "Molecular Simulations Shed Light on Supersoft Elasticity in Polydomain Liquid Crystal Elastomers," *Macromolecules*, vol. 47, pp. 8824–8832, Dec. 2014.

[70] N. A. Traugutt, D. Mistry, C. Luo, K. Yu, Q. Ge, and C. M. Yakacki, "Liquid-Crystal-Elastomer-Based Dissipative Structures by Digital Light Processing 3D Printing," *Advanced Materials*, vol. 32, no. 28, p. 2000797, 2020.

[71] H. Wermter and H. Finkelmann, "Liquid crystalline elastomers as artificial muscles," *e-Polymers*, vol. 1, Dec. 2001.

[72] T. H. Ware and T. J. White, "Programmed liquid crystal elastomers with tunable actuation strain," *Polymer Chemistry*, vol. 6, no. 26, pp. 4835–4844, 2015.

[73] W. Fan, Z. Wang, and S. Cai, "Rupture of Polydomain and Monodomain Liquid Crystal Elastomer," *International Journal of Applied Mechanics*, vol. 08, p. 1640001, Oct. 2016.

[74] N. Hill and M. Haghi, "Deposition direction-dependent failure criteria for fused deposition modeling polycarbonate," *Rapid Prototyping Journal*, vol. 20, pp. 221–227, Jan. 2014.

[75] H. Rezayat, W. Zhou, A. Siriruk, D. Penumadu, and S. S. Babu, "Structure–mechanical property relationship in fused deposition modelling," *Materials Science and Technology*, vol. 31, pp. 895–903, June 2015.

[76] M. Barnes, S. M. Sajadi, S. Parekh, M. M. Rahman, P. M. Ajayan, and R. Verduzco, "Reactive 3D Printing of Shape-Programmable Liquid Crystal Elastomer Actuators," *ACS Applied Materials & Interfaces*, vol. 12, pp. 28692–28699, June 2020.

[77] H. Yuk and X. Zhao, "A New 3D Printing Strategy by Harnessing Deformation, Instability, and Fracture of Viscoelastic Inks," *Advanced Materials*, vol. 30, no. 6, p. 1704028, 2018.

[78] A. Kotikian, R. L. Truby, J. W. Boley, T. J. White, and J. A. Lewis, "3D Printing of Liquid Crystal Elastomeric Actuators with Spatially Programed Nematic Order," *Advanced Materials*, vol. 30, no. 10, p. 1706164, 2018.

[79] D. J. Roach, X. Kuang, C. Yuan, K. Chen, and H. J. Qi, "Novel ink for ambient condition printing of liquid crystal elastomers for 4D printing," *Smart Materials and Structures*, vol. 27, p. 125011, Nov. 2018.

[80] M. O. Saed, C. P. Ambulo, H. Kim, R. De, V. Raval, K. Searles, D. A. Siddiqui, J. M. O. Cue, M. C. Stefan, M. R. Shankar, and T. H. Ware, "Molecularly-Engineered, 4D-Printed Liquid Crystal Elastomer Actuators," *Advanced Functional Materials*, vol. 29, no. 3, p. 1806412, 2019.

[81] C. P. Ambulo, J. J. Burroughs, J. M. Boothby, H. Kim, M. R. Shankar, and T. H. Ware, "Four-dimensional Printing of Liquid Crystal Elastomers," *ACS Applied Materials & Interfaces*, vol. 9, pp. 37332–37339, Oct. 2017.

[82] D. J. Broer, H. Finkelmann, and K. Kondo, "In-situ photopolymerization of an oriented liquid-crystalline acrylate," *Die Makromolekulare Chemie*, vol. 189, no. 1, pp. 185–194, 1988.

[83] D. Trivedi, C. D. Rahn, W. M. Kier, and I. D. Walker, "Soft robotics: Biological inspiration, state of the art, and future research," *Applied Bionics and Biomechanics*, vol. 5, pp. 99–117, Jan. 2008.

[84] D. Rus and M. T. Tolley, "Design, fabrication and control of soft robots," *Nature*, vol. 521, pp. 467–475, May 2015.

[85] L. Hines, K. Petersen, G. Z. Lum, and M. Sitti, "Soft Actuators for Small-Scale Robotics," *Advanced Materials*, vol. 29, no. 13, p. 1603483, 2017.

[86] A. D. Marchese, R. Tedrake, and D. Rus, "Dynamics and trajectory optimization for a soft spatial fluidic elastomer manipulator," *The International Journal of Robotics Research*, vol. 35, pp. 1000–1019, July 2016.

[87] C. D. Onal and D. Rus, "Autonomous undulatory serpentine locomotion utilizing body dynamics of a fluidic soft robot," *Bioinspiration & Biomimetics*, vol. 8, p. 026003, Mar. 2013.

[88] A. D. Marchese, C. D. Onal, and D. Rus, "Autonomous Soft Robotic Fish Capable of Escape Maneuvers Using Fluidic Elastomer Actuators," *Soft Robotics*, vol. 1, pp. 75–87, Feb. 2014.

[89] A. A. Stokes, R. F. Shepherd, S. A. Morin, F. Ilievski, and G. M. Whitesides, "A Hybrid Combining Hard and Soft Robots," *Soft Robotics*, vol. 1, pp. 70–74, July 2013.

[90] S. J. A. Koh, X. Zhao, and Z. Suo, "Maximal energy that can be converted by a dielectric elastomer generator," *Applied Physics Letters*, vol. 94, p. 262902, June 2009.

[91] C. Keplinger, T. Li, R. Baumgartner, Z. Suo, and S. Bauer, "Harnessing snap-through instability in soft dielectrics to achieve giant voltage-triggered deformation," *Soft Matter*, vol. 8, no. 2, pp. 285–288, 2012.

[92] A. Lendlein and R. Langer, "Biodegradable, Elastic Shape-Memory Polymers for Potential Biomedical Applications," *Science*, vol. 296, pp. 1673–1676, May 2002.

[93] O. Medina, A. Shapiro, and N. Shvalb, "Kinematics for an Actuated Flexible n-Manifold," *Journal of Mechanisms and Robotics*, vol. 8, Apr. 2016.

[94] A. Zolfagharian, A. Kaynak, and A. Kouzani, "Closed-loop 4D-printed soft robots," *Materials & Design*, vol. 188, p. 108411, Mar. 2020.

[95] T. Kim, S. J. Yoon, and Y. Park, "Soft Inflatable Sensing Modules for Safe and Interactive Robots," *IEEE Robotics and Automation Letters*, vol. 3, pp. 3216–3223, Oct. 2018.

[96] M. Yamada, M. Kondo, R. Miyasato, Y. Naka, J.-i. Mamiya, M. Kinoshita, A. Shishido, Y. Yu, C. J. Barrett, and T. Ikeda, "Photomobile polymer materials—various three-dimensional movements," *Journal of Materials Chemistry*, vol. 19, no. 1, pp. 60–62, 2009.

[97] M. Rogóż, H. Zeng, C. Xuan, D. S. Wiersma, and P. Wasylczyk, "Light-Driven Soft Robot Mimics Caterpillar Locomotion in Natural Scale," *Advanced Optical Materials*, vol. 4, no. 11, pp. 1689–1694, 2016.

[98] S. Palagi, A. G. Mark, S. Y. Reigh, K. Melde, T. Qiu, H. Zeng, C. Parmeggiani, D. Martella, A. Sanchez-Castillo, N. Kapernaum, F. Giesselmann, D. S. Wiersma, E. Lauga, and P. Fischer, "Structured light enables biomimetic swimming and versatile locomotion of photoresponsive soft microrobots," *Nature Materials*, vol. 15, pp. 647–653, June 2016.

[99] P.-G. D. Gennes, M. Hébert, and R. Kant, "Artificial muscles based on nematic gels," *Macromolecular Symposia*, vol. 113, no. 1, pp. 39–49, 1997.

[100] D. K. Shenoy, D. Laurence Thomsen III, A. Srinivasan, P. Keller, and B. R. Ratna, "Carbon coated liquid crystal elastomer film for artificial muscle applications," *Sensors and Actuators A: Physical*, vol. 96, pp. 184–188, Feb. 2002.

[101] M.-H. Li and P. Keller, "Artificial muscles based on liquid crystal elastomers," *Philosophical Transactions of the Royal Society A: Mathematical, Physical and Engineering Sciences*, vol. 364, pp. 2763–2777, Oct. 2006.

[102] R. S. Kularatne, H. Kim, J. M. Boothby, and T. H. Ware, "Liquid crystal elastomer actuators: Synthesis, alignment, and applications," *Journal of Polymer Science Part B: Polymer Physics*, vol. 55, no. 5, pp. 395–411, 2017.

[103] M. López-Valdeolivas, D. Liu, D. J. Broer, and C. Sánchez-Somolinos, "4d printed actuators with soft-robotic functions," *Macromolecular rapid communications*, vol. 39, no. 5, p. 1700710, 2018.

[104] S. Gantenbein, K. Masania, W. Woigk, J. P. Sesseg, T. A. Tervoort, and A. R. Studart, "Three-dimensional printing of hierarchical liquid-crystal-polymer structures," *Nature*, vol. 561, no. 7722, pp. 226–230, 2018.

[105] V. Schöppner and K. P. KTP, "Mechanical properties of fused deposition modeling parts manufactured with ultem* 9085," in *Proceedings of 69th Annual Technical Conference of the Society of Plastics Engineers (ANTEC'11)*, vol. 2, pp. 1294–1298, 2011.

[106] O. S. Carneiro, A. F. Silva, and R. Gomes, "Fused deposition modeling with polypropylene," *Materials & Design*, vol. 83, pp. 768–776, Oct. 2015.

[107] C. P. M. Linares, N. A. Traugutt, M. O. Saed, A. M. Linares, C. M. Yakacki, and T. D. Nguyen, "The effect of alignment on the rate-dependent behavior of a main-chain liquid crystal elastomer," *Soft Matter*, vol. 16, no. 38, pp. 8782–8798, 2020.

[108] S. Akbari, A. H. Sakhaei, K. Kowsari, B. Yang, A. Serjouei, Z. Yuanfang, and Q. Ge, "Enhanced multimaterial 4d printing with active hinges," *Smart Materials and Structures*, vol. 27, no. 6, p. 065027, 2018.

[109] Y. Mao, K. Yu, M. S. Isakov, J. Wu, M. L. Dunn, and H. J. Qi, "Sequential self-folding structures by 3d printed digital shape memory polymers," *Scientific reports*, vol. 5, no. 1, pp. 1–12, 2015.

[110] Y. Liu, B. Shaw, M. D. Dickey, and J. Genzer, "Sequential self-folding of polymer sheets," *Science Advances*, vol. 3, no. 3, p. e1602417, 2017.

VITA

ZOZEF SIDDIQUI

Candidate for the Degree of

Master of Science

Thesis: STRUCTURE-PROPERTY RELATIONSHIPS IN 4D-PRINTED LIQUID CRYSTAL ELASTOMERS

Major Field: Mechanical and Aerospace Engineering

Biographical:

Education:

Completed the requirements for the Bachelor of Science in Mechanical Engineering at Bangladesh University of Engineering and Technology, Dhaka, Bangladesh in 2017.

Experience:

Employed by Oklahoma State University, School of Mechanical and Aerospace Engineering as a graduate research and teaching assistant from 2019 to 2021